Proteomic analysis of Rhodospirillum rubrum after carbon monoxide exposure reveals an important effect on metallic cofactor biosynthesis

Christine Cavazza, Véronique Collin-Faure, Julien Pérard, Hélène Diemer, Sarah Cianférani, Thierry Rabilloud, Elisabeth Darrouzet

This work has been originally published in Journal of Proteomics under the doi 10.1016/j.jprot.2021.104389.
This version may not include all the final corrections made after acceptance of the manuscript

Proteomic analysis of *Rhodospirillum rubrum* after carbon monoxide exposure reveals an important effect on metallic cofactor biosynthesis

Christine Cavazza[a], Véronique Collin-Faure[a], Julien Pérard[a], Hélène Diemer[b,c], Sarah Cianférani[b,c], Thierry. Rabilloud[a,*] and Elisabeth. Darrouzet[a,*]

[a]CEA, CNRS, Université Grenoble Alpes, IRIG, CBM, F-38000 Grenoble, France
christine.cavazza@cea.fr; veronique.collin@cea.fr; julien.perard@cea.fr; thierry.rabilloud@cnrs.fr; elisabeth.darrouzet@cea.fr

[b]Laboratoire de Spectrométrie de Masse BioOrganique (LSMBO), Université de Strasbourg, CNRS, IPHC UMR 7178, 67000 Strasbourg, France

[c]Infrastructure Nationale de Protéomique ProFI – FR2048 (CNRS-CEA), 67087 Strasbourg, France

hdiemer@unistra.fr; sarah.cianferani@unistra.fr;

*Co-last authors and corresponding authors.

Conflicts of interest

The authors declare that they have no conflict of interest.

Acknowledgments

This work was supported by the Agence Nationale de la Recherche through the LabEx ARCANE program (ANR-11-LABX-0003-01) and the Graduate School on Chemistry, Biology and Health of Univ Grenoble Alpes CBH-EUR-GS (ANR-17-EURE-0003).

This work was supported by the CNRS, the University of Strasbourg, the "Agence Nationale de la Recherche" and the French Proteomic Infrastructure (ProFI; ANR-10-INBS-08-03).

We would like to thanks Umberto Contaldo for its help with CODH activities measurements.

Abstract

Some carboxydotrophs like *Rhodospirillum rubrum* are able to grow with CO as their sole source of energy using a Carbone monoxide dehydrogenase (CODH) and an Energy conserving hydrogenase (ECH) to perform anaerobically the so called water-gas shift reaction (WGSR) ($CO + H_2O \rightarrow CO_2 + H_2$). Several studies have focused at the biochemical and biophysical level on this enzymatic system and a few OMICS studies on CO metabolism. Knowing that CO is toxic in particular due to its binding to heme iron atoms, and is even considered as a potential antibacterial agent, we decided to use a proteomic approach in order to analyze *R. rubrum* adaptation in term of metabolism and management of the toxic effect. In particular, this study allowed highlighting a set of proteins likely implicated in ECH maturation, and important perturbations in term of cofactor biosynthesis, especially metallic cofactors. This shows that even this CO tolerant microorganism cannot avoid completely CO toxic effects associated with its interaction with metallic ions.

Significance

This proteomic study highlights the fact that even in a microorganism able to handle carbon monoxide and in some way detoxifying it via the intrinsic action of the carbon monoxide dehydrogenase (CODH), CO has important effects on metal homeostasis, metal cofactors and metalloproteins. These effects are direct or indirect via transcription regulation, and amplified by the high interdependency of cofactors biosynthesis.

1. Introduction

Purple nonsulfur photosynthetic bacteria such as *Rhodospirillum rubrum* (*R. rubrum*) are particularly interesting for biotechnological applications owing to their great versatility in term of metabolism. They are able to grow aerobically or anaerobically in the dark, photosynthetically in the absence of oxygen, autotrophically or heterotrophically using a wide variety of substrates and electron acceptors. In particular, *R. rubrum* has been selected by the European Space Agency (ESA) for its photo-assimilation of volatile fatty acids in the bio-regenerative life support system (MELiSSA) aimed at recycling gas and solid wastes during long distance space flights [1]. Besides, *R. rubrum* is also highly interesting due to its ability under anaerobic conditions to directly produce H_2 from CO as sole energy source via the water-gas shift reaction (WGSR) ($CO + H_2O \rightarrow CO2 + H_2$) that is linked to ATP production [2]. In biotechnological applications, this metabolism is also used to produce polyhydroxyalkanoates (PHA), the yield of which is highly increased by the addition of other carbon sources like acetate, in the dark or with light [3]. In this organism, acetate can be assimilated via three different routes: the citrate malate cycle, the ethylmalonyl-CoA pathways and a pathway implicating the ferredoxin-dependent pyruvate synthase (PFOR) [3, 4]. However, this bacterium cannot grow with acetate alone and requires a source of energy such as light. When CO is added (for example with syngas), it can be used as a carbon and energy source in a rather additive manner [3].

Microbial utilization of CO appears more and more common in bacteria or archaea, either in aerobic or anaerobic conditions and, depending on the microorganism, allows the production of hydrogen, methane, ethanol, butanol, acetic or butyric acid as well as carbon assimilation into biomass (proteins, biopolymers such as PHA…). Several studies have focused at the biochemical and biophysical level on the essential enzymatic system involved in WGSR in hydrogenogenic carboxydotrophs species such as *R. rubrum* or *Carboxydothermus hydrogenoformans*. This multiprotein complex is composed of two key nickel enzymes: a monofunctional [NiFe]-carbon monoxide dehydrogenase (CODH), which catalyzes CO oxidation to CO_2, releasing electrons used for the reduction of two protons to yield H_2, the latter reaction being catalyzed by a CO-tolerant membranous energy-conserving [NiFe]-hydrogenase (ECH). This CO-oxidizing complex contains also CooF, a ferredoxin that transfers electrons from CODH to hydrogenase. The genes coding for these proteins are clustered in two operons: the *cooMKLXUH* operon coding for ECH and downstream, the *cooFSCTJ* operon encoding the ferredoxin CooF, the CODH CooS and three maturation proteins, namely CooC, Coo T and CooJ involved in nickel insertion into the CODH active site [5-7]. These two operons are under the control of the heme-dependent CO-sensing transcriptional activator CooA present downstream the cooFSCTJ operon.

However, no global approach (transcriptomics, proteomics, metabolomics) have focused on the identification of other potential maturation factors (hydrogenase maturation, synthesis and insertion of the iron sulfur clusters…).

In organometallic chemistry, CO binding to transition metals is well known. Indeed, CO is a good ligand for π-electron-rich metals. It is an unsaturated soft ligand able to donate σ-electrons to the metal and to accept metal dπ-electrons by back bonding. Coordination complexes can be formed directly from CO gas and metal but often require a reducing agent when starting from the metal salt or oxide. For example in aqueous buffer, nickel or cobalt salts can be reduced by sodium dithionite and form in presence of CO the homoleptic complexes $Ni(CO)_4$ or $Co(CO)_4^-$. Another example among the multitude includes formation of mixed complexes like $Mg(O_3)_2(CO)_2$, a neutral magnesium carbonyl complex with CO binding to the Mg^{2+} center [8]. In biology, binding of CO to metal in porphyrin-like structures is common with the probably best-known example being CO binding to heme and especially to hemoglobin as it is the case in CO intoxication. Other examples include cobalt porphyrin which is none other than a derivative of cobalamin or vitamin B12, and the example cited above of mixed magnesium complex suggests that even chlorophyll derivatives with their magnesium ion might be affected [9]. CO is also able to bind to copper like in tyrosinase or hemocyanin and this binding is even used as a tool to investigate O_2 interactions [10]. In addition, CO also affects iron-sulfur with labile position or with a [3Fe-4S] cluster like in aconitase, fumarase or glutamate synthase, or more complex

clusters in nitrogenases, NiFe or iron only hydrogenases [11-15]. All this suggests that in theory, most if not all transition metals used in biological systems could be the target of CO if a labile position is present in their coordination sphere. The susceptibility of all these cofactors to CO (and the stability of the complex formed) is going to be protein dependent in term of CO access, metal coordination sphere (nature and arrangement) and metal oxidation state that is often in equilibrium and changes during electron transfer mechanisms.

CO is well known for its toxic effect and several studies based on omic approaches have focused on its ability to act as an antibacterial agent in particular with CO releasing molecules (CORM) [16-18]. The role of CO as a key signaling molecule especially in higher eukaryotes is also well documented suggesting a more complex action [19] and a parallel is done between NO and CO as detailed in Watts *et al.* 's review [20]. Indeed these two molecules have similar chemical properties especially in term of binding affinity to transition metal and mode of coordination (both acting as π acidic ligand). Data on NO interactions at the molecular level are much more documented and for example, NO is able to mobilize iron from ferritin perturbing intracellular iron homeostasis [21].

Consequently, a class of proteins going to have a broader impact if affected are transcriptional regulators. Indeed several of them act as (or are associated with) gaseous ligand sensors, metal, cellular redox poise or aerobic/anaerobic conditions through a mechanism often based on heme, iron-sulfur cluster or mononuclear metal binding. As a few examples, one can cite CooA or RcoM regulation by CO (which is their main physiological role), Zur, Nur and Fur regulation by Zn^{2+}, Ni^{2+} and Fe^{2+}, respectively, redox poise / oxygen/ oxidative stress sensing by heme (FixLJ) or iron-sulfur cluster (IscR, SoxRS system) [22-26]. Interaction of CO with the metal ions may perturb all the proteins they regulate. For example, Fur regulates at least 90 proteins in *E. coli* [27] and transcriptomics studies with CORM derivatives in *E. coli* have indeed highlighted Fur activity perturbation.

Nevertheless, several bacteria including the hydrogenogenic carboxydotroph *Rhodospirillum rubrum* are able to grow with CO as their unique source of energy and/or carbon source. We therefore performed a proteomic study in order to analyze

i) *R. rubrum* metabolic adaptation including the induction of CODH and its maturation machinery, a CO resistant hydrogenase as well as potential yet unidentified maturation proteins
ii) its management of the general toxic effect of CO interaction with metals in comparison with non-carboxydotrophs.

2. Materials and methods

2.1. Strain and Culture conditions

The *R. rubrum* strain UR2 used in this study was a kind gift from L.M. Rubio. Glycerol stocks were aerobically grown in 5 mL of MN medium supplemented with 3g/L of yeast extract and 3 g/L of casamino acids to give the SMN medium (adapted from [28]) for several days at 30°C, 180 rpm. *R.rubrum* UR2 was then grown under anaerobic photoheterotrophic conditions in 50 mL malate ammonium (MN) medium in gas-tight flasks for 4 days. These anaerobic cultures were used to inoculate ten 15 mL-cultures in RRNCO medium (2 µg of biotin,
2.8 mg of H_3BO_3, 20 mg of Na_2EDTA, 4 mg of ferric citrate, 1 mg of Na_2MoO_4, 250 mg of $MgSO_4$.7H2O, 132 mg of $CaCl_2$.2H2O, 1 g of NH_4Cl, .6 mg of $NiCl_2$, 1.0 g of yeast extract, 2.1 g of morpholinopropanesulfonic acid (MOPS), and 0.82 g of sodium acetate per liter, pH 7.1) at 30°C under photoheterotrophic conditions in 30 mL-flasks [29]. When the $OD_{660\ nm}$ reached about 1.0 (corresponding to the stationary phase in these conditions), 50 µM $NiSO_4$ and 500 µM Na_2S were added to all cultures (adapted from [29]) as the enzyme CODH and the ECH hydrogenase are supposed to be highly induced upon CO exposure, and require Ni and sulfur in their metallic clusters. Note that Na_2S also warrants a reductive environment. Five cultures were then sparged with CO for 30 min at t_0 and t_{19h} (and left with an initial small overpressure < 1 bar), after addition of 125 µM

$NaHCO_3$ pH 8.0. 24h after CO exposure, the ten cultures (+/- CO) were harvested by centrifugation (5 000 rpm, 20 min), and frozen in liquid nitrogen. For activity measurement, at the end of the culture, samples of 1 ml or 5 ml were centrifuged, the supernatant discarded and the pellet frozen in liquid nitrogen.

2.2. Activity measurements

2.2.1. CO oxidation activities

CO oxidation measurements on "whole fresh cells" were performed as a control of the correct CO-induction of the *cooFSCTJ* operon. 5 µL of cell culture were injected in gas-tight cuvettes containing 1 mL of CO-saturated 100 mM MOPS pH 7.5, 12 mM methyl viologen and 1 mM DTT. CODH activity was assayed at 25 °C in triplicates, by following the reduction of methyl viologen at 604 nm [ε=13.6 mM^{-1} cm^{-1}. CODH activity unit is expressed as nanomoles of CO oxidized per minute.
For measurement on "frozen roughly permeabilized cells", cell pellets from 1 ml samples were resuspended with 100 µL of buffer (TrisHCl 50 mM, DTT 10 mM, dithionite 10 mM, pH 8.5; final volume around 145 µL). 1,5 µL from each sample was injected into 1 mL of buffer TrisHCl 50 mM, Methyl Viologen 12 mM, DTT 1 mM, saturated with CO. Measures were performed on three different cultures for each condition and in triplicate for CO induced.

2.2.2. Hydrogenase activity measurement

Cell pellets from 5 ml samples were resuspended in a glovebox by addition of 100 µL of BugBuster® Protein Extraction Reagent (Millipore) and 350 µL of TrisHCl 50 mM pH 8.5 buffer (final volume around 550 µL). 20 µL from CO exposed and 50 µL from control samples were injected into 1 mL of TrisHCl 50 mM Methyl Viologen 12 mM, DTT 1 mM, saturated with H_2. Measures were performed in triplicate.

2.2.3. 3-hydroxybutyrate dehydrogenase activity measurement

Cell pellets from 5 ml samples were resuspended with the equivalent of 66 µL per mL culture DO 1 of BugBuster® Protein Extraction Reagent (Millipore) and incubated 1 h at room temperature. Samples were then centrifuged at 15 000 rpm during 30 minutes, and the supernatants frozen until further use. 500 µL of Buffer (HEPES 100mM pH 7,6; MgCl2 10mM ; KCl 100mM ; Triton X-100 2%, preheated at 37°C), 370 µl of water (preheated at 37°C), 10 µl of a mix 1/1 freshly prepare phenazine methosulfate (6 mM in DMSO)/iodonitrotetrazolium (20 mg/ml in DMSO), 60 µL of NAD^+ at 20 mg/ml and 50 µL of soluble fractions of each sample were mixed in a 1 mL cuvette.
NADH formation is measured indirectly by following at 500 nm the tetrazolium salt reduction resulting in the formation of a red formazan. After 3 minutes stabilisation the background is measured (ΔDO/min). 10 µL of substrate 3-hydroxybutyrate 1 M are added and the slope recorded between 300 and 400 s. Measures were performed in duplicate on 3 different cultures for each condition.

2.3. Protein extraction and quantification

The washed bacterial pellets were extracted with 200 µl of lysis solution (7 M urea, 2 M thiourea, 15 mM spermine base, 15 mM spermine tetrahydrochloride, 10 mM Tris (carboxyethyl) phosphine hydrochloride and 2% (w/v) Brij96). This detergent was selected for its ability to extract membrane proteins [30]. After extraction at room temperature for one hour, the extracts were clarified by centrifugation (15000 g 15 minutes), the supernatants collected and their protein concentration determined by a modified Bradford assay [31]. The protein extracts were stored frozen at -20°C until use.

2.4. Shotgun approach

For the shotgun proteomic analysis, the samples were included in polyacrylamide plugs according to Muller *et al.*, with some modifications to downscale the process [32]. To this purpose, the photopolymerization system using methylene blue, toluene sulfinate and diphenyliodonium chloride was used [33].
First, a sample dilution solution (8M urea in 200mM Tris HCl, pH 8) was prepared. Then, the dye solution (0.5 mM methylene blue in sample dilution solution) was prepared. The other initiator solutions consisted in a 1 M solution of sodium toluene sulfinate in water and in a saturated water solution of diphenyliodonium chloride. The ready-to-use polyacrylamide solution consisted of 1.2 ml of a commercial 40% acrylamide/bis solution (37.5/1) to which 100 µl of diphenyliodonium chloride solution, 100 µl of sodium toluene sulfinate solution and 100 µl of water were added.
Protein samples (30 µg each) were first diluted to a 5 µl final volume with sample dilution solution in a 500 µl conical microtube (Eppendorf). To this solution, 4 µl of dye solution then 3 µl of acrylamide solution were then added and mixed by pipetting. 100 µl of water-saturated butanol were then layered on top of the samples, and polymerization was carried out under a 1500 lumen 2700K LED lamp for 2 hours, during which the initially blue gel solution discolored. At the end of the polymerization period, the butanol was removed, and the gel plugs were fixed for 2x1 hr with 200 µl of 30% ethanol 2 % phosphoric acid, followed by a 30 minutes wash in 30% ethanol. The fixed gel plugs were then stored at -20°C until use.

2.5. 2D gel analysis

Two-dimensional electrophoresis was performed essentially as described previously, using homemade pH 4-8 pH gradients in the first dimension and a 11.5% polyacrylamide gel (160x200x1.5 mm) operating at pH 8.05 with the taurine system in the second dimension [34, 35]. This system allowed an easy analysis of low molecular weight proteins, as described earlier [35]. 150 µg of proteins were loaded on the first dimension IPG gel. Protein detection and image analysis were performed as described previously [36]. Spots were selected for further mass spectrometry analysis if their U value in the Mann-Whitney U test was ≤2 in the control vs. +CO comparison. No threshold filter was applied, as this has been shown to lead to discarding relevant data [37].

2.6. Mass spectrometry analysis

2.6.1. 2D gel-based proteomics

In gel washing, reduction, alkylation and dehydration were performed with a robotic protein handling system (MassPrep Station, Waters, Milford, USA). The gel plugs were washed twice with 50 µL of 25 mM ammonium hydrogen carbonate (NH_4HCO_3) and 50 µL of acetonitrile. The cysteine residues were reduced by 50 µL of 10 mM dithiothreitol at 57°C and alkylated by 50 µL of 55 mM iodoacetamide. After dehydration with acetonitrile, the proteins were cleaved in gel with 10 µL of 6.5 ng/µL of modified porcine trypsin (Promega, Madison, WI, USA) in 25 mM NH_4HCO_3. The digestion was performed overnight at room temperature. The generated peptides were extracted with 40 µL of 60% acetonitrile in 0.1% formic acid. Acetonitrile was evaporated under vacuum and samples were resuspended with 6 µL of 0.1% formic acid.
NanoLC-MS/MS analysis was performed using a nanoACQUITY Ultra-Performance-LC (Waters Corporation, Milford, USA) coupled to the TripleTOF 5600 (Sciex, Ontario, Canada).
The nanoLC system was composed of ACQUITY UPLC® CSH130 C18 column (250 mm x 75 µm with a 1.7 µm particle size, Waters Corporation, Milford, USA) and a Symmetry C18 precolumn (20 mm × 180 µm with a 5 µm particle size, Waters Corporation, Milford, USA). The solvent system consisted of 0.1% formic acid in water (solvent A) and 0.1% formic acid in acetonitrile (solvent B). 4 µL of sample were loaded into the enrichment column during 3 min at 5 µL/min with 99% of solvent

A and 1% of solvent B. Elution of the peptides was performed at a flow rate of 300 nL/min with a 8-35% linear gradient of solvent B in 9 minutes.
The TripleTOF 5600 (Sciex, Ontario, Canada) was operated in positive mode, with the following settings: ionspray voltage floating (ISVF) 2300 V, curtain gas (CUR) 10, interface heater temperature (IHT) 150, ion source gas 1 (GS1) 2, declustering potential (DP) 80 V. Information-dependent acquisition (IDA) mode was used with Top 10 MS/MS scans. The MS scan had an accumulation time of 250 ms on m/z [400;1250] range and 100 ms on m/z [150;1800] range in high sensitivity MS/MS mode. Switching criteria were set to ions with charge state of 2-4 and an abundance threshold of more than 500 counts, exclusion time was set at 4 s. IDA rolling collision energy script was used for automatically adapting the CE. Mass calibration of the analyzer was achieved using peptides from digested BSA. The complete system was fully controlled by AnalystTF 1.7 (Sciex). Raw data collected were processed and converted with MSDataConverter in .mgf peak list format.
For protein identification, the MS/MS data were interpreted using a local Mascot server with MASCOT 2.6.2 algorithm (Matrix Science, London, UK) against an in-house database containing all *Rhodospirillum rubrum* entries from UniProtKB/SwissProt (version 2019_12, 3,985 sequences) and the corresponding 3,985 reverse entries. The database was generated using the database toolbox from Mass Spectrometry Data Analysis (MSDA, publicly available from https://msda.unistra.fr). Spectra were searched with a mass tolerance of 15 ppm for MS and 0.07 Da for MS/MS data, allowing a maximum of one trypsin missed cleavage. Trypsin was specified as enzyme. Carbamidomethylation of cysteine residues and oxidation of methionine residues were specified as variable modifications. Protein identifications were validated with at least two peptides with Mascot ion score above 30.

2.6.2. Shotgun proteomics

In gel washing, reduction, alkylation and dehydration were performed with a robotic protein handling system (MassPrep Station, Waters, Milford, USA). The gel plugs were washed twice with 50 µL of 25 mM ammonium hydrogen carbonate (NH_4HCO_3) and 50 µL of acetonitrile. The cysteine residues were reduced by 50 µL of 10 mM dithiothreitol at 57°C and alkylated by 50 µL of 55 mM iodoacetamide. After dehydration with acetonitrile, the proteins were cleaved in gel with 10 µL of 70 ng/µL of modified porcine trypsin (Promega, Madison, WI, USA) in 25 mM NH_4HCO_3. The digestion was performed overnight at room temperature. The generated peptides were extracted with 40 µL of 60% acetonitrile in 0.1% formic acid. Acetonitrile was evaporated under vacuum and samples were resuspended with 78 µL of 0.1% formic acid in order to obtain a final concentration of 450 ng/µL.
NanoLC-MS/MS analysis was performed using a nanoACQUITY Ultra-Performance-LC (Waters Corporation, Milford, USA) coupled to a Q-Exactive Plus mass spectrometer (Thermo Fisher Scientific, Bremen, Germany).
The nanoLC system was composed of ACQUITY UPLC® CSH130 C18 column (250 mm x 75 µm with a 1.7 µm particle size, Waters Corporation, Milford, USA) and a Symmetry C18 precolumn (20 mm × 180 µm with a 5 µm particle size, Waters Corporation, Milford, USA). The solvent system consisted of 0.1% formic acid in water (solvent A) and 0.1% formic acid in acetonitrile (solvent B).
300 ng of peptides sample was loaded into the enrichment column during 3 min at 5 µL/min with 99% of solvent A and 1% of solvent B. Elution of the peptides was performed at a flow rate of 450 nL/min with a 1-35% linear gradient of solvent B in 79 minutes.
The Q-Exactive Plus was operated in data-dependent acquisition mode by automatically switching between full MS and consecutive MS/MS acquisitions. Full-scan MS spectra were collected from 300 - 1,800 m/z at a resolution of 70,000 at 200 m/z with an automatic gain control target fixed at 3×10^6 ions and a maximum injection time of 50 ms. The top 10 precursor ions with an intensity exceeding 2×10^5 ions and charge states ≥ 2 were selected from each MS spectrum for fragmentation by higher-energy collisional dissociation. Spectra were collected at a resolution of 17,500 at 200 m/z with a fixed first mass of 100 m/z, an automatic gain control target fixed at 1×10^5 ions and a maximum injection time of 100 ms. Dynamic exclusion time was set to 60 s. Raw data were converted into mgf files using the MSConvert tool from ProteomeWizard (v3.0.6090; http://proteowizard.sourceforge.net/).

For protein identification, the MS/MS data were interpreted using a local Mascot server with MASCOT 2.6.2 algorithm (Matrix Science, London, UK) against the previously described in-house database. Spectra were searched with a mass tolerance of 10 ppm for MS and 0.07 Da for MS/MS data, allowing a maximum of one trypsin missed cleavage. Trypsin was specified as enzyme. Acetylation of protein n-termini, carbamidomethylation of cysteine residues and oxidation of methionine residues were specified as variable modifications. Identification results were imported into Proline software (http://proline.profiproteomics.fr/) for validation. Peptide Spectrum Matches (PSM) with pretty rank equal to one were retained. False Discovery Rate was then optimized to be below 1% at PSM level using Mascot Adjusted E-value and below 1% at Protein Level using Mascot Mudpit score.

2.6.3. Label Free Quantification

Peptides Abundances were extracted thanks to Proline software version 2.0 (http://proline.profiproteomics.fr/) using a m/z tolerance of 10 ppm. Alignment of the LC-MS runs was performed using Loess smoothing. Cross Assignment was performed within groups only. Protein Abundances were computed by sum of peptides abundances (normalized using the median).
Proteins were considered as significantly different if their U value in the Mann-Whitney U test was ≤ 2 in the control vs. +CO comparison. No threshold filter was applied, as this has been shown to lead to discarding relevant data [37].

2.7. Pathways analysis

KEGG Mapper – Search Pathway tool was used to map on various metabolic pathways the proteins identified by mass spectrometry in our study [38]. The pathways are general pathways onto which the proteins theoretically present (genome based) in *R. rubrum* are usually highlighted in green rectangles with an added red border for the list of identified proteins with no weighting option. Filtering was performed before generating the Tables. All the proteins in **Supplementary Table 1 and 4** were therefore used as proteins present in the proteome and all the proteins in **Supplementary Table 2 and 4** as up or down-regulated ones. Up and down-regulated proteins were analyzed separately. The data have then been combined and color coded to yield a single figure for each pathway. The analysis was completed by bibliographic study especially for protein not included in pathways.

2.8. ICP-AES metal ion analysis

15 ml of *R. rubrum* culture exposed or not to CO were centrifuged at 5000 rpm for 10 minutes. 5.4 ml of the supernatant were mineralized in the presence of 0,6 ml nitric acid (65%) at 60°C for 1hour. The cell pellet was washed in PBS supplemented with 10 mM EDTA before being lysed and mineralized with 1.2ml of 65% nitric acid for 3h at 60°C; the volume was completed to 6 mL with pure water. Metal concentration was analyzed by inductively coupled plasma atomic emission spectroscopy (ICP-AES) (Shimadzu ICP 9000 with mini plasma torch in axial reading mode). Standard solutions of Ni, Co, Mo, Mg, and Fe for atomic absorption spectroscopy (Sigma Aldrich) were used for quantification (calibration curve between 1.9 to 5000 $\mu g\ L^{-1}$ in 10% HNO3 (Fluka)). The analyses were performed on three cultures from each condition (with or without CO) and each result was normalized to the number of bacteria as estimated from the OD at 650nm.

3. Results and discussion

3.1. Proteome of *R. rubrum* grown under anaerobic light conditions

Shotgun experiments on cell extracts from *R. rubrum* grown with acetate under anaerobic light conditions allowed us to identified 1572 non-redundant proteins (**Table 1 in Supplementary Data**) which represents around 41% of the 3852 predicted proteins including 50 encoded on a megaplasmid

(or more than 39% of the 3985 sequences found in UniprotKB database). This number is considerably higher than the proteomic study performed on this organism by Mastroleo *et al.* in 2009 who identified 932 non-redundant proteins for cultures in aerobic dark conditions. This is of the same order as the 1725 proteins identified by Leroy *et al.* in 2015 in a study aiming at understanding acetate photoassimilation in *R. rubrum* or the 1823 proteins identified by Bayon-Vicente *et al.* in 2020 for *R. rubrum* grown on acetate or succinate, with various amounts of bicarbonate and varying light intensity [4, 39, 40]. Comparing our data with the study of Leroy *et al.*, 573 proteins are encountered only in our study and 726 in theirs and comparing with the recent study of Bayon *et al.*, around 730 proteins are found only in one of the studies (241 only in our study and 592 in theirs). Therefore, combining the four studies allows the confirmation of the expression of two-thirds of the proteins predicted from the genome, but in very different physiological conditions. Moreover four additional proteins (Q2RMU9, Q2RWT0, Q2RX52 and Q2RSA0), not detected in our shotgun approach were identified following a 2D approach (see below).
As shown in **Supplementary Figure 1 and 2** for example carbon metabolism or amino-acid synthesis, which are essential pathways using abundant proteins, are extremely well covered.

3.2. Comparative proteomic studies of *R. rubrum* exposed or not to carbon monoxide: shotgun approach

Anaerobic cultures of *R.rubrum* growing in the light with acetate were sparged or not with CO gas upon a period of 24 hours. It was chosen to start with an early stationary phase in order to minimize the important metabolic changes occurring during exponential /stationary phase transition. Among the 1572 protein identified both with and without CO, 435 were differentially expressed considering a Mann–Whitney U test inferior or equal to 2, corresponding in the experimental scheme to a p-value below 0.05. More precisely, 187 proteins were up-regulated and 248 down-regulated (**Supplementary Table 2**)

3.3. Comparative proteomic studies of *R. rubrum* exposed or not to carbon monoxide: 2DE approach

Mass spectrometry analysis after 2DE is a complementary approach to direct shotgun. Indeed, some proteins are not easily detected in shotgun but most importantly, 2DE approach allows the detection of proteins regulated at the posttranslational level whereas their total amount may be stable.
The same extracts as those used for the shotgun experiment were used for the 2DE approach and 2200 spots were detected on average on the different gels. The aim of this experiment being to identify differently modulated proteins after CO exposure and not to determine *R. rubrum* proteome, only significantly-varying spots (U test ≤ 2) plus spots suspected to correspond to post-translationally modified forms of varying proteins were selected, cut and analyzed (**Figure 1A and 1B, and Supplementary Figure 3 and 4** for the complete set of gels (control and CO exposed cultures, respectively). The quantitative data for 2D gels analysis are also presented in **Supplementary Table 3.** The 98 significantly varying spots plus one invariant corresponded to 77 non-redundant proteins, 10 proteins being identified from 2 different spots and 6 from 3 different spots. 27 proteins are up-regulated and 46 proteins down-regulated plus 4 proteins that are both up or down-regulated depending on the spots from which they have been identified (**Supplementary Table 4**).

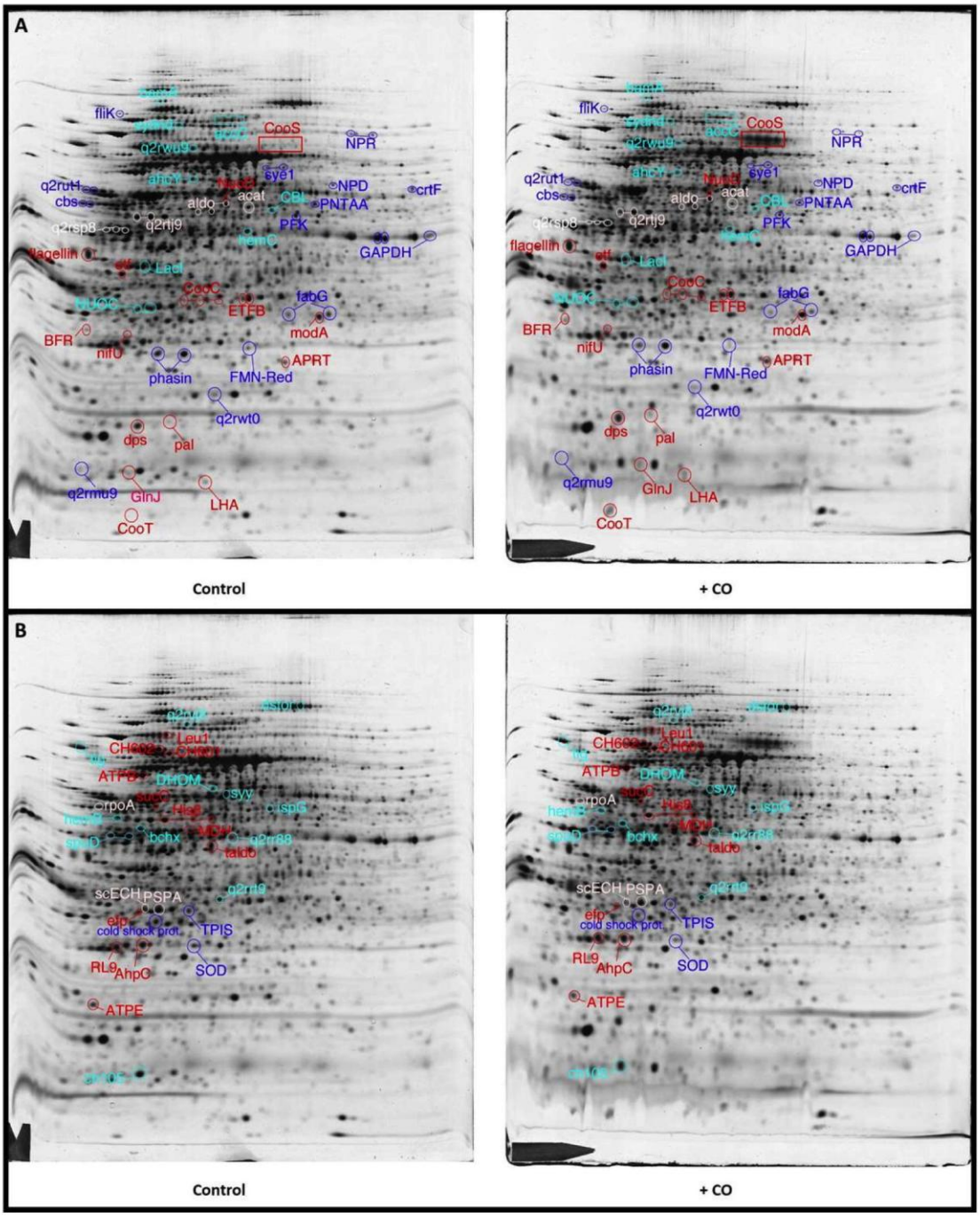

Figure 1: Figure 1 Panels A and B: Proteomic analysis of total cell extracts by 2D electrophoresis
Total cell extracts of R. rubrum cells were separated by two-dimensional gel electrophoresis. The first dimensions covered a 4-8 pH range and the second dimension a 5-200 kDa range. Total cellular proteins (150 µg) were loaded on the first dimension gel. Spots that are significantly changed in their intensities by exposure to CO are shown. The colors have been chosen only for legibility purposes. The splitting of the figure in two parts has also been made only for legibility purposes.

3.4. Pathways analysis

The KEGG mapper tool was used to analyze more precisely the pathways or sub-pathways in which the varying proteins are implicated. **Supplementary Table 5** summarizes the number of proteins up and down-regulated as well as the number of proteins detected (full proteome). In the categories Metabolic pathways (rru01100), Biosynthesis of secondary metabolites (rru01110), Microbial

metabolism in diverse environments (rru01120), Carbon metabolism (rru01200) and Biosynthesis of amino acids (rru01230) we found almost twice less up-regulated than down-regulated proteins, suggesting a strong impact of CO on the global metabolism.

3.4.1. Central metabolism

Carbon metabolism

Concerning carbon metabolism, the proteins are associated for example with Pyruvate metabolism (rru00620), Carbon fixation in photosynthetic organisms (rru00710), Glyoxylate and dicarboxylate metabolism (rru00630), Propanoate and Butanoate metabolism (rru00640). Regarding the latter pathway, Polyhydroxyalkanoates (PHA) and in particular polyhydroxybutyrates (PHB) are used by many bacteria as a carbon and energy storage molecule [41]. When needed PHBs are mobilized to give back acetyl-CoA. This metabolism is connected to butanoate metabolism. With CO, four enzymes implicated in PHB synthesis from acetyl-CoA (Q2RXR6 (Acetyl-CoA acetyltransferase), Q2RXR7 (3-oxoacyl-[acyl-carrier-protein] reductase), Q9RDT6 (PHA synthase) and Q2RRN2 (Poly(R)-hydroxyalkanoic acid synthase, class I)) are down-regulated at least in one of our approaches (**See Figure 2**) (See **Table 1** for a list of the varying proteins discussed in the text).

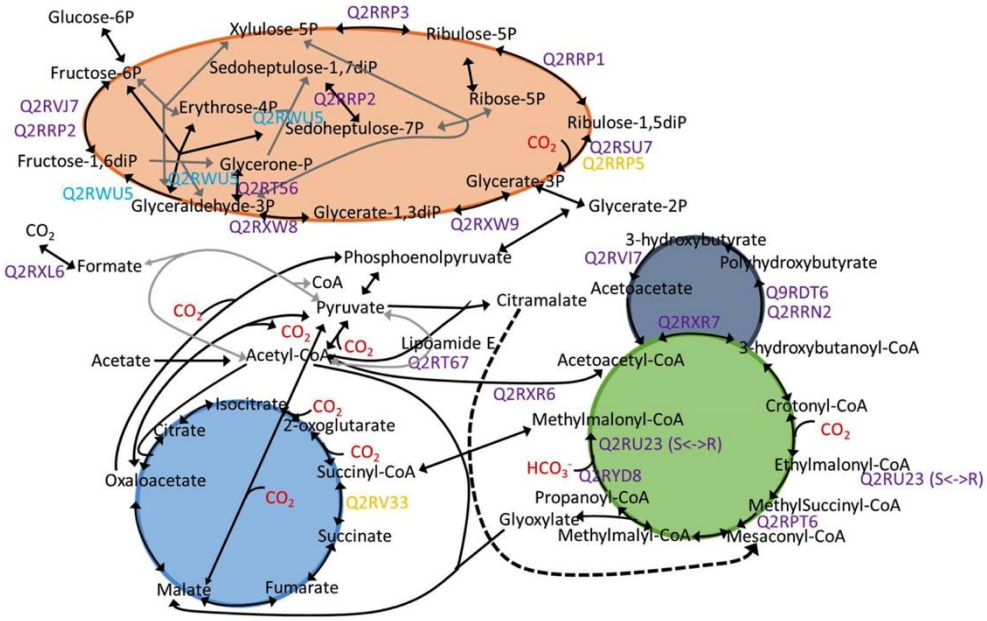

Figure 2: main metabolic network of *R. rubrum* central carbon metabolism

The proteins upregulated after CO exposure are written in orange and the ones downregulated in purple. The protein Q2RWU5 (Fructose-1,6-bisphosphate aldolase) is identified in three different spots varying in opposite direction on 2D gels and is written in cyan

Table 1: List of proteins significantly modulated by CO exposure and discussed in the manuscript. For the complete lists of proteins regulated by CO and identified by shotgun or 2D gel based proteomic analyses see **Supplementary Table 2 and 4**, respectively.

accession	description	ratio CO/ ctrl	p value	coverage (%)	# peptides	Shotgun or 2D gel
P31894	Iron-sulfur protein CooF	2,23E+07	6,16E-05	45	10	Shotgun
P31895	Carbon monoxide-induced hydrogenase	1,48E+08	2,38E-05	66	26	Shotgun
P31896	Carbon monoxide dehydrogenase	2,37E+03	9,77E-06	93	67	Shotgun
P31896	Carbon monoxide dehydrogenase	2,70E+01	<E-04	32	17	2D Gel
P31896	Carbon monoxide dehydrogenase	2,60E+01	<E-04	37	18	2D Gel
P31896	Carbon monoxide dehydrogenase	1,16E+02	<E-04	35	18	2D Gel
P31897	Carbon monoxide dehydrogenase accessory protein CooC	9,64E+07	1,05E-04	71	18	Shotgun
P31897	Carbon monoxide dehydrogenase accessory protein CooC	3,73E+00	<E-04	39	9	2D Gel
P31897	Carbon monoxide dehydrogenase accessory protein CooC	2,93E+00	<E-04	39	9	2D Gel
P31897	Carbon monoxide dehydrogenase accessory protein CooC	1,74E+00	4,80E-03	24	6	2D Gel
P72316	CooM	1,76E+06	3,65E-02	3	3	Shotgun
P72317	CooL	1,52E+07	3,87E-04	63	8	Shotgun
P72318	CooX	8,41E+06	5,52E-04	54	7	Shotgun
P72319	CooU	2,11E+07	1,03E-04	72	14	Shotgun
P72320	CooT	2,22E+07	6,53E-04	61	3	Shotgun
P72320	CooT	2,13E+01	2,50E-03	61	3	2D Gel
P72321	CooJ	2,54E+07	2,06E-04	42	4	Shotgun
P72322	CooA	8,28E+06	5,23E-05	32	7	Shotgun
P77937	CooK	1,81E+06	4,48E-02	5	2	Shotgun
Q2RMQ6	Transcriptional regulator, BadM/Rrf2 family	8,20E-01	4,11E-02	30	4	Shotgun
Q2RMQ8	Molybdopterin biosynthesis protein	5,22E-01	3,58E-03	26	5	Shotgun
Q2RMR3	Ferric uptake regulation protein	2,18E+00	6,32E-05	19	3	Shotgun
Q2RMS8	CBS domain protein	1,14E+00	2,35E-02	22	7	2D Gel
Q2RMS8	CBS domain protein	7,88E-01	2,90E-03	21	7	2D Gel
Q2RNH0	Nitrogen-fixing NifU-like	1,51E+00	7,05E-04	35	5	Shotgun
Q2RNH0	Nitrogen-fixing NifU-like	5,39E-01	1,40E-03	39	7	2D Gel
Q2RP67	Phasin	1,11E+00	5,50E-02	65	11	2D Gel
Q2RP67	Phasin	7,80E-01	2,60E-03	61	9	2D Gel
Q2RPC9	Uncharacterized protein	1,08E+06	2,34E-05	21	3	Shotgun
Q2RPD0	TonB-dependent receptor	1,98E+01	2,70E-04	60	29	Shotgun
Q2RPD1	Twin-arginine translocation pathway signal	3,44E+05	1,17E-02	13	2	Shotgun
Q2RQL4	Basic membrane lipoprotein	6,02E-01	2,85E-04	61	13	Shotgun
Q2RR75	Iron-regulated ABC transporter membrane component SufB	1,15E+00	3,37E-02	29	9	Shotgun
Q2RR76	FeS assembly ATPase SufC	1,79E+00	1,23E-02	32	8	Shotgun
Q2RR78	Cysteine desulfurase	1,41E+00	7,28E-05	53	14	Shotgun
Q2RRH6	FeoA	6,29E+00	9,21E-06	42	3	Shotgun
Q2RRN2	Poly(R)-hydroxyalkanoic acid synthase, class I	4,57E-01	4,09E-05	49	22	Shotgun
Q2RRP5	Ribulose bisphosphate carboxylase	1,26E+00	2,93E-02	49	15	Shotgun
Q2RSN8	Molybdopterin-guanine dinucleotide biosynthesis MobB region	6,86E-01	5,17E-02	34	5	Shotgun
Q2RSU7	5-methylthioribulose-1-phosphate isomerase	7,72E-01	3,95E-04	17	4	Shotgun
Q2RT62	Magnesium transport protein CorA	3,56E-01	1,95E-02	6	2	Shotgun
Q2RTI5	Superoxide dismutase	6,42E-01	5,00E-04	23	5	2D Gel
Q2RU10	Putative depolymerase	6,66E-01	1,69E-02	19	4	Shotgun
Q2RU56	Molybdenum-pterin binding protein	1,66E+01	1,72E-03	61	2	Shotgun

Q2RUE4	Transcriptional regulator, ArsR family	1,98E+00	2,15E-03	8	2	Shotgun
Q2RUV7	Trimethylamine-N-oxide reductase (Cytochrome c)	5,75E-01	1,89E-02	50	33	2D Gel
Q2RUW0	Cytoplasmic chaperone TorD	4,00E+00	3,06E-08	60	9	Shotgun
Q2RVI7	3-hydroxybutyrate dehydrogenase	4,50E-01	3,10E-03	19	4	Shotgun
Q2RVS8	Xanthine dehydrogenase, molybdenum binding subunit apoprotein	3,86E-01	5,42E-03	6	4	Shotgun
Q2RVZ1	Pyruvate formate-lyase	1,57E+00	5,16E-02	4	3	Shotgun
Q2RWI7	Molybdenum ABC transporter, periplasmic binding protein	1,83E+00	2,88E-04	59	14	Shotgun
Q2RWI7	Molybdenum ABC transporter, periplasmic binding protein	1,29E+00	2,70E-03	50	11	2D Gel
Q2RWQ9	Chemotaxis sensory transducer	4,31E-01	2,71E-03	4	2	Shotgun
Q2RWU5	Fructose-1,6-bisphosphate aldolase	1,37E+00	1,10E-03	11	4	2D Gel
Q2RWU5	Fructose-1,6-bisphosphate aldolase	8,53E-01	2,80E-03	36	14	2D Gel
Q2RWU5	Fructose-1,6-bisphosphate aldolase	6,16E-01	4,00E-04	30	10	2D Gel
Q2RWU9	Extracellular solute-binding protein, family 5	7,69E-01	4,30E-03	19	11	2D Gel
Q2RXL6	Formate dehydrogenase alpha subunit	7,26E-01	2,02E-02	49	25	Shotgun
Q2RXM7	Aldehyde ferredoxin oxidoreductase	9,03E+00	8,85E-03	4	2	Shotgun
Q2RXN2	Carbamoyltransferase HypF	3,66E+00	2,92E-06	16	6	Shotgun
Q2RXN4	Hydrogenase maturation factor	8,33E+00	4,06E-07	40	9	Shotgun
Q2RXN5	Hydrogenase expression/formation protein HypE	6,55E+01	5,06E-06	49	13	Shotgun
Q2RXR6	Acetyl-CoA acetyltransferase	7,59E-01	2,80E-03	63	18	2D Gel
Q2RXR7	3-oxoacyl-[acyl-carrier-protein] reductase	8,24E-01	2,00E-03	60	11	2D Gel
Q2RXR7	3-oxoacyl-[acyl-carrier-protein] reductase	7,30E-01	2,30E-03	44	8	2D Gel
Q9RDT6	PHA synthase	4,63E-01	6,34E-05	30	15	Shotgun

Q2RWU9 (Extracellular solute-binding protein, family 5) and Q2RQL4 (Basic membrane lipoprotein) are two proteins associated with PHB granules and are up and down-regulated, respectively [42]. On the other hand, PHB degradation involves in particular an activator of depolymerisation Phasin and a depolymerase [43]. In our study, Phasin (Q2RP67) has 2 spots which vary in opposite direction in 2DE approach and the more acidic one (likely the modified form) is down regulated in the presence of CO. The protein Q2RVI7 (3-hydroxybutyrate dehydrogenase) also implicated in the PHB cycle (**Figure 2**) is down-regulated and a loss of activity (3-hydroxybutyrate + NAD^+ gives acetoacetate + NADH + H^+) has been confirmed experimentally on cell extracts (**Table 2**). We also detected Q2RU10 (Putative depolymerase, PhaZ1) as down-regulated but contrary to PhaZ2 (Q2RNZ5) this protein is supposed to be periplasmic [44]. *R. rubrum* seems therefore to have decreased or stopped its PHB synthesis and use. This is quite different from Revelles *et al*.'s study in which they exposed *R. rubrum* to syngas (a mixture of CO, CO_2 and H_2) and still observed PHB synthesis as probed by isotope labelling [3]. Yet, the syngas they used is composed of 40% CO whereas we sparged our culture with pure CO and an initial small overpressure (<1 bar).

Table 2: Enzymatic activity measurement. Measurements were performed as stated in the Materials and Methods section. The values correspond to the activity of 1 mL culture normalized to 1 OD.

	Mean control	Standard deviation control	Mean CO	Standard deviation CO	CO / control	t test
3-hydroxybutyrate dehydrogenase activity (nmoles of hydroxybutyrate oxidized min^{-1})	6.5	0,61	4.2	0.29	0.65	0.0009
CODH activity (nmol of CO oxidized min^{-1})	2.43	0,38	1005	62	413	2.10E-08
Hydrogenase activity (nmoles of H2 oxidized min^{-1})	0	0	1.2	0.29		

Ribulose 1,5-biphosphate carboxylase (Q2RSU7, 5-methylthioribulose-1-phosphate isomerase) protein is also down-regulated suggesting that CO_2 fixation decreased after exposure to high CO concentration. However, another protein (Q2RRP5, Ribulose bisphosphate carboxylase) also annotated as Rubisco, is on the contrary upregulated (**Figure 2**). Pyruvate-flavodoxin oxidoreductase (Q53046, PFOR) also implicated in CO_2 fixation is invariant
A protein annotated as pyruvate formate lyase (Q2RVZ1, PFL) is up-regulated but the formate dehydrogenase H subunit alpha (Q2RXL6) the activity of which is known to be CO sensitive is down-regulated.

CO related metabolism, enzymes involved in WGSR

It is well known that CODH is overproduced after CO exposure in *R. rubrum*. As a control CO oxidation activity was therefore directly checked on whole cells at the end of the culture. The activities were about 0 and 300 U/mL for the negative controls and the CO-exposed cultures, respectively (1 U = 1 nmole CO oxidized per min). In our shotgun study we can observe that CooS (P31896, Carbon monoxide dehydrogenase), CooF (P31894, Iron-sulfur protein) and the six proteins of the hydrogenase complex (CooM (P72316), CooK (P77937), CooL (P72317), CooX (P72318), CooU (P72319) and CooH (P31895, Carbon monoxide-induced hydrogenase)) are indeed largely produced after CO exposure as well as the CO-responsive transcription factor CooA (P72322) (see **Figure 3** for *coo* operon and CODH/ECH complex). Note that CooA is a transcription activator, the activity of which is enhanced by conformational changes triggered by CO binding to its heme so its regulatory function does not necessarily imply a change in protein level [45]. The proteins CooS is also significantly increased on 2D gels.

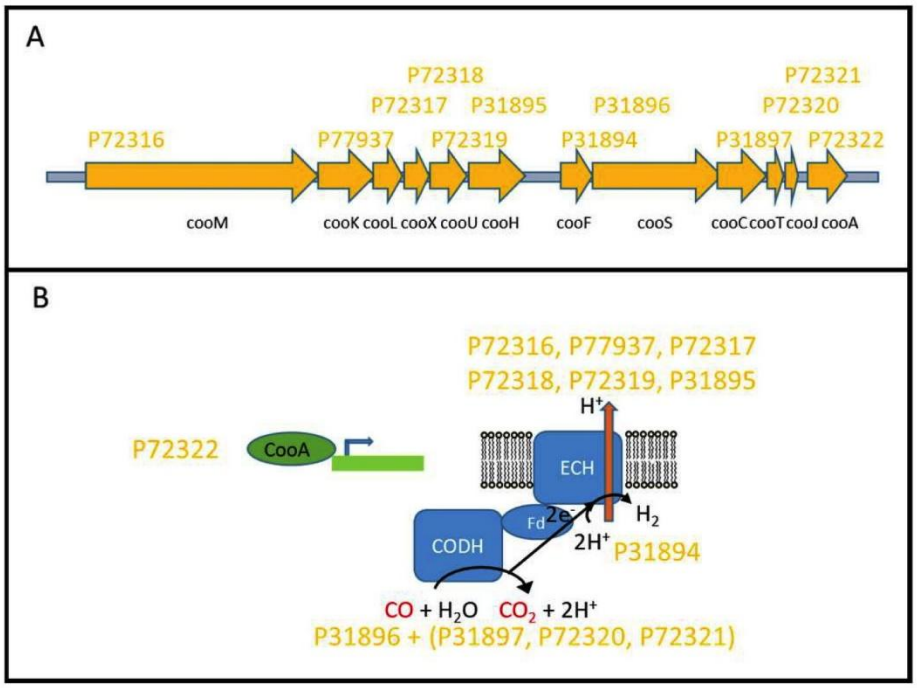

Figure 3 : R. rubrum coo cluster and the corresponding proteins
Panel A : the cooMKLXUH and cooFSCTJ operons are represented as well as cooA encoding the CO responsive transcription regulator acting on the two coo operons. Corresponding protein names are written above the sequence. All the proteins associated are up-regulated.
Panel B : Schematic view of Coo proteins implicated in the water-gas shift reaction : the Carbon monoxide dehydrogenase (CODH), its maturation proteins, transcription regulator as well as the CO induced energy conserving hydrogenase (ECH).

CODH dimer possesses three classical Fe_4S_4 clusters and two atypical $NiFe_4S_4$ clusters forming the active sites. The active site biosynthesis is a multistep process that starts with the insertion of Fe and S atoms, to form a Fe_4S_4 cluster, likely performed by the Suf machinery and it is worth noting that the Suf machinery is indeed induced after CO exposure. The following step is the insertion of the Ni atom thanks to the three nickel-binding proteins: CooC (P31897), CooT (P73320) and CooJ (P73321) that are greatly induced in shotgun analysis and also in 2D gel approach for CooC and CooT, and this despite the large excess of nickel present in the growth media. Another interesting point deals with the different spots observed on 2D gels for CooS (P31896) and CooC, highlighting post-translational modifications with all forms increased. However, a more specific study will be required to determine precisely the nature of these modifications

Three different [NiFe]-hydrogenases have been described in *R. rubrum*: the CO-linked ECH involved in WGSR, a formate-linked hydrogenase and a H_2 uptake hydrogenase. The six subunits of the CO-linked ECH are highly up-regulated, only two proteins (Q2RXM4 and Q2RXM2) of the formate-linked hydrogenase are detected and are invariant, and no protein were detected for the uptake hydrogenase Hup (**Figure 4**).

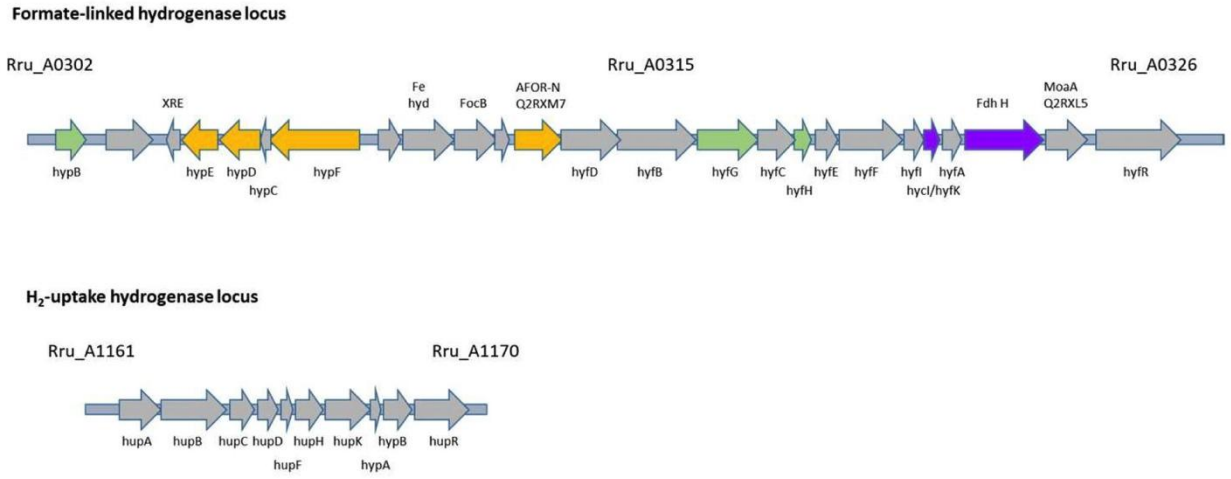

Figure 4: *R. rubrum* formate-linked and uptake hydrogenase locus.
Grey, green, orange and purple arrows represents genes encoding proteins that are respectively not detected, invariant, up-regulated or down-regulated after CO exposure.
The gene names below the clusters correspond to *Escherichia coli* or *Pectobacterium atrosepticum* denomination for the formate-linked hydrogenase (pyruvate formate-lyase) and to *Rhodobacter capsulatus* denomination for the H_2-uptake hydrogenase [48, 52].
Above the cluster of the formate-linked hydrogenase are the names of the encoded proteins: XRE :transcriptional regulator XRE family;
Fe hyd : [FeFe] hydrogenase; FocB: formate transporter; AFOR-N: Aldehyde ferredoxin oxidoreductase; FdhH: formate dehydrogenase; MoaA: GTP 3',8-cyclase.

As for CODH, the biosynthesis of [Ni-Fe]-hydrogenase active site is a multistep process involving at least six strictly conserved accessory proteins, namely HypABCDEF, in addition to a specific protease cleaving the C-terminal tail (HycI in *E. coli*, HyfK in *Pectobacterium atrosepticum*) [46-48]. In some bacteria such as *Rubrivivax gelatinosus*, *hyp* genes potentially responsible for CO-induced ECH maturation are clustered next and among the *coo* genes [49]. This is not the case for *R. rubrum* but searching for homologies, we could find four clustered genes *hypE* (Q2RXN5), *hypD* (Q2RXN4), *hypC* (Q2RXN3) and *hypF* (Q2RXN2) in close proximity to the gene cluster encoding the formate-linked hydrogenase (**Figure 4**). While the hydrogenase in this cluster does not seem to be up-regulated (2 invariant proteins detected), the HypDEF proteins are highly up-regulated (HypC was also found up-regulated but being identified with a single peptide, it has been discarded) after CO exposure. This

tends to show that in *R. rubrum* the same maturation machinery would be used for both formate-linked hydrogenase and ECH maturation while the H_2-uptake enzyme possesses its own maturation machinery (**Figure 4**). Besides, it suggests the existence of a co-regulation mechanism between ECH and the HypCDEF proteins expression. There is next to the four hyp genes a XRE family transcriptional regulator (Q2RXN6) but its function cannot be determined by homology. On the other hand, looking at the genomic sequence upstream of hypF, it was possible to find a CooA binding site similar to the ones determined for the CODH and ECH operons (**Figure 4**) [50, 51]. *R. rubrum* possesses two hypA and two hypB paralogs. One hypA and one hypB belongs to the H_2 uptake hydrogenase Hup cluster (**Figure 4**) and the corresponding proteins are not detected [52]. The other hypA gene is isolated and its protein not detected, and the second hypB is located in the formate-lyase cluster and the protein is invariant. However, HypA and HypB are both involved in nickel insertion into [NiFe]-hydrogenases and in *E. coli* at least, these two proteins are dispensable when high nickel concentration is present.
CODH and hydrogenase activities were checked on permeabilized cells and cell lysate, respectively in order to back up the proteomics results (**Table 2**).

3.4.2. Metal metabolism and regulation

Our proteomic study revealed that different proteins implicated in the homeostasis of various transition metals such as iron, nickel, cobalt or molybdenum were perturbed by CO exposure.

Metal Transporters and sensors
Q2RRH6 (FeoA) is largely up-regulated (6 folds). The feoA gene is followed by one gene homologous among others to feoB from *E coli*, and preceded by one annotated also as feoA but which is not homologous at least to feoA from *E. coli*. FeoA is implicated in ferrous iron transport and is regulated in *E. coli* by the metalloregulator Ferric Uptake Regulator (Fur) controlling iron acquisition systems and the fumarate and nitrate reduction regulator (FNR) controlling the aerobic/anaerobic transition in facultative anaerobes, Fe being mainly present as Fe^{2+} under anoxygenic conditions [53, 54].
Q2RPD1 (Twin-arginine translocation pathway signal) is a periplasmic iron siderophore/cobalamin-binding protein ABC transporter. It is homologous to *E. coli* ferrichrome ABC transporter/ iron(III) hydroxamate binding protein (encoded by *fhuD*), to the ferric enterobactin-binding periplasmic protein (encoded by *fepB*), and to vitamin B12 (cyano-cobalamin) (encoded by *btuF*). Q2RPD0 (TonB-dependent receptor) is a TonB-dependent outer membrane transport system that typically acts in series with the above permeases. Q2RPD0 is homologous to FecA (ferric citrate transport protein), BtuB, FepA, or FhuA for example, all associated with iron or cobalt transport. Q2RPC9 (Uncharacterized protein) is an uncharacterized protein annotated as a Fe transport with no strong homology with any known protein, and contains a DUF2478 domain that is often found in proteins near the molybdenum ABC transporter (MobA, MobB and MobC). These three clustered proteins are all highly up-regulated ($3.5\ 10^5$, 20 and $1.1\ 10^6$ folds, respectively). One can note that the following genes (Rru_A3222 and Rru_A3223) encode for proteins (Q2RPC8 (Transport system permease protein) and Q2RPC7 (ABC transporter component)) not detected in our experiment but corresponding to the permease membranous domain and the ATP binding subunit, respectively. BtuF gene is usually isolated in the genome whereas on the contrary fhu and fep genes are very often organized in operons with the other subunits of the permease (membrane component and ATP binding subunit) like this is the case here, suggesting that this is indeed one of these two iron chelated transport systems which is up-regulated [55].
The protein Q2RU56 (Molybdenum-pterin binding protein) annotated as a molybdate transporter is highly up-regulated and the ModA (Q2RWI7, Molybdenum ABC transporter, periplasmic binding protein) transporter of molybdate is also slightly up-regulated both in shotgun and 2DE experiments (1.8 and 1.3 folds, respectively).
Q2RMS8 (CBS domain protein) is homologous to CorC from *E. coli* (CorC-HlyC family), with the same genomic context (apolipoprotein, PhoH-like downstream). It contains a FAD binding site and is

annotated in *E. coli* as a magnesium and cobalt efflux protein [56-58]. In our study, we observed one spot up and the other down-regulated (1.1 and 0.8 folds, respectively) suggesting a change in the level of post-translational modification of this subunit upon CO exposure.
Q2RT62 protein (Magnesium transport protein CorA) is down-regulated (0.35 folds). CorA is a primary Mg^{2+} transporter which also mediates non specific import of Ni^{2+} and Co^{2+} [59]. Like in *R. rubrum*, the gene for CorA protein stands alone in the genome of *E. coli* or *Shigella flexneri* even if it works in a transporter system in association with other Cor proteins including CorC [56].
It is worth noting that several ABC transporters predicted to transport metallic ions also varied after CO exposure but the nature of the metal is hardly identifiable by using homology predictions.
One can note that the protein NikA (Q2RS18) belonging to the nickel transport system and detected in our study is invariant in agreement with the study of Watt and Ludden that showed that Ni-import is CO-independent [60].
Chemotaxis sensory transducer like Q2RWQ9 (chemotaxis methyl-accepting receptor) has a hemerythrin-like domain and is down regulated after CO exposure.

Regulators
Several transcription factors regulating metal homeostasis are affected by CO exposure.
The Fur-like family includes several metal uptake regulation proteins such as Fur (for Fe(II) uptake), (Nur (for Ni(II) uptake), Zur (for Zn(II) uptake) or Mur (for Mn(II) uptake), as well as the Irr (iron response regulator) and the H_2O_2-sensing regulator PerR. In the family, three metallic sites can be encountered (a metal specific sensing site, an accessory metal-binding site often occupied by Zn^{2+} and a structural binding site), but they are not all always present. Moreover, the ligands may vary (in amino acid identity and position) between the different classes but also sometimes in the same functional class making the classification challenging [22, 61]. *R. rubrum* genome encodes three proteins of the Fur family: Q2RMT4 and Q2RT34 that are invariant and not detected, respectively, and the up-regulated Q2RMR3 (2.2 folds). As shown on the alignment sequence (**Figure 5**) performed with well-characterized members of the different classes, we can postulate that Q2RMT4 and Q2RT34 are Fur and Zur proteins, respectively [62-65]. Concerning Q2RMR3, even if it is highly homologous to the atypical PerR from *Leptospira interrogans* devoid of a structural metal-binding site, it seems that it is rather an Irr protein as suggested as well by phylogenetic analyses in alpha-proteobacteria [66-69]. Most of the time, the Fur-like family proteins regulate the intracellular concentration of metals and some proteins containing these metals [61, 69]. For example, Nur regulates the *nikABCD*E gene operon (nickel transporter) in *Streptomyces coelicolor*, represses the FeSOD and induces the NiSOD in the presence of nickel [23]. Irr proteins are distinct in the way that they sense heme and not directly Fe^{2+} iron. Here like Irr in *Rhizobium leguminosarum*, the protein does not have the N-terminal heme regulatory motif (HRM) but only internal histidine residues [67]. Irr proteins are quite unstable and rapidly degraded when heme is present especially when the HRM motif is present [70]. When the HRM site is absent, heme binding rather promotes oligomerization and impedes DNA binding and hence prevents the repressor capacity of Irr [71]. On the contrary, for Fur the presence of iron promotes its binding to DNA.

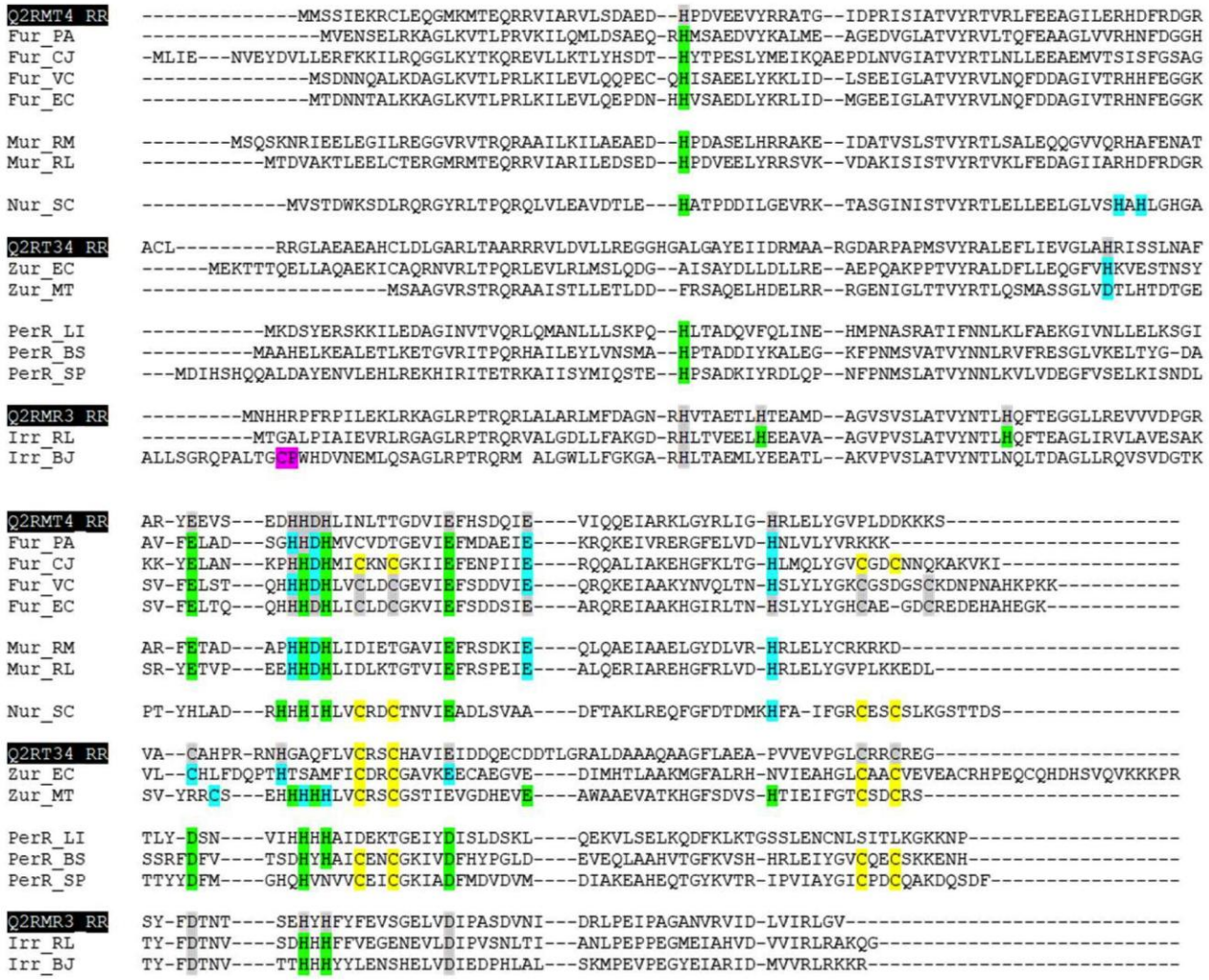

Figure 5 : Sequence alignment of Fur-like proteins.
Q2RMT4_RR, Q2RT34_RR and Q2RMR3_RR: the three Fur-like proteins from Rhodospirillum rubrum. Fur_PA Pseudomonas aeruginosa(Q03456); Fur_CJ Campylobacter jejuni (P0C631); Fur_VC Vibrio cholerae (A5F6G4); Fur_EC Escherichia coli (P0A9A9); Mur_RM Rhizobium meliloti (Q92LL6); Mur_RL Rhizobium leguminosarum (O07315); Nur_SC Streptomyces coelicor (Q9K4F8); Zur_EC Escherichia coli (P0AC51); Zur_MT Mycobacterium tuberculosis (P9WN85); PerR_Li Leptospira interrogans (Q72QS5); PerR_BS Bacillus subtilis (P71086); PerR_SP Streptomyces pyogenes (P72567); Irr_RL Rhizobium leguminosarum (Q8KLU1); Irr_BJ Bradyrhizobium japonicum (O85719).
Green, cyan and yellow indicates the amino acid residues experimentally shown to be implicated in metal binding and grey conserved ones. Green metal sensing site cyan accessory site and yellow the cysteine residues implicated in the structural site or disulfide bridge. For Irr, the magenta indicate CP in the HRM motif (Heme regulatory motif) that binds heme but is not always conserved and green the His residues implicated in heme binding. [62-67, 69, 102-107].

Q2RUE4 (Transcriptional regulator, ArsR family) (the protein is also annotated now as a Protein-tyrosine-phosphatase) is up-regulated (2 folds). Genes downstream encode for proteins annotated as arsenite transporter, and then arsenical resistance operon transacting repressor ArsD and arsenite transporting ATPase which is invariant. The same genomic organization is present in some other bacteria. ArsR/smtB-like repressors bind to the operator/promoter and seem to dissociate in the presence of metal ions, allowing transcription of the proteins generally involved in metal-ions efflux and/or detoxification. The arsR/smtB family includes transcription repressors responsive to Ag^{1+}, Cu^{1+}, Cd^{2+}, Co^{2+}, Ni^{2+}, Pb^{2+}, Zn^{2+}, As^{3+}, and Bi^{3+}.

There are “Cross-homologies” between proteins from different species and the metal type sense by these regulators or transport proteins is difficult to identify. Besides, for this type of regulator, their status (loaded or not loaded with metal) is probably more meaningful than the raw amount of protein.

Metallic ions content

In order to strengthen our hypothesis that CO has perturbed metal homeostasis we proceeded to ICP-AES quantification. As shown in **Table 3**, after CO exposure, iron and molybdenum are significantly increased and decreased in the bacteria, respectively. Concerning iron, this increased intracellular accumulation even resulted in a partial depletion of the medium. For molybdenum, the proportion of intracellular metal compared to the medium is not high enough to have a visible effect on culture medium concentration. The higher iron accumulation correlates well with the increased of several iron transporter and storage molecules as detected by proteomics.

Table 3 :ICP-AES measurements. Measurements were performed as stated in the Materials and Methods section. An equivalence of 10^9 bacteria per 1 OD_{650} was used.

Concentration in µM in the supernatants	Mean control	Standard deviation control	Mean CO	Standard deviation CO	Ratio CO/ctrl	t test
Co	0,15	0,034	0,18	0,040	1,25	0,30
Mg	1930	77	1900	92,4	0,98	0,67
Fer	24,6	1,7	19,1	1,15	0,78	0,01
Mo	5,5	0,44	4,8	0,60	0,87	0,17
Ni	30,4	7,9	40,3	2,9	1,33	0,15
Cu	0,03	0,000	0,03	0,010	0,83	0,42
Zn	0,95	0,045	0,79	0,080	0,83	0,05
Mn	0,07	0,012	0,07	0,012	1,00	1,00
Metal in the cells (nmoles of ions/10^9 bacteria)	Mean control	Standard deviation control	Mean CO	Standard deviation CO	Ratio CO/ctrl	t test
Co	0,022	0,006	0,016	0,002	0,69	0,20
Mg	53,3	5,06	41,2	7,1	0,77	0,08
Fer	2,4	0,068	4,3	0,39	1,78	0,01
Mo	0,20	0,012	0,11	0,015	0,57	0,00
Ni	0,20	0,094	0,13	0,009	0,63	0,31
Cu	0,016	0,006	0,019	0,003	1,19	0,48
Zn	0,11	0,008	0,12	0,008	1,10	0,16
Mn	0,000	0,000	0,000	0,000		

3.4.3. Cofactors biosynthesis

Proteins modulated by the CO exposure are involved in various cofactors biosynthetic pathways. One can cite: i) Carotenoid biosynthesis (rru00906) (**Supplementary Figure 5**) with 3 proteins down-regulated, ii) Ubiquinone and other terpenoid-quinone biosynthesis (rru00130) (**Supplementary Figure 6**) with 2 down and 1 up-regulated proteins, iii) Porphyrin and chlorophyll metabolism (rru00860) (8 down and 2 up-regulated proteins including one up-regulated in the shotgun experiment but down-regulated in the 2 DE one with 2 spots) (**Supplementary Figure 7**), and iv) Riboflavin metabolism (rru00740) (**Supplementary Figure 8**) with 5 down-regulated proteins out of the 7 detected in our experiments.

Porphyrin and chlorophyll metabolism

Focusing on the porphyrin and chlorophyll metabolisms (**Supplementary Figure 7**), the down regulated proteins map mainly on the beginning of heme synthesis and probably up to uroporphyrinogen III, the branching point to the cobalamin (vitamin B12) pathway. The end of the heme synthesis pathway and the chlorophyll part seems much less affected. Remarkably, chlorophyll implicates a Mg porphyrin contrary to the classical heme that binds Fe, which is a good target for CO binding.

Cobalamin synthesis

Concerning cobalamin synthesis, two pathways historically identified as aerobic (cob) and anaerobic (cbi) exist in bacteria [72]. However, the distinction is not so clear-cut. Some bacteria possess both, but for example in *R. rubrum*, the cbi pathway is incomplete and the cob pathway is able to function even in the absence of oxygen in particular with the flavoprotein CobZ [73]. Along the complete pathway starting from amino-levulinate, 5 proteins are down-regulated. (**Supplementary Figure 7**). Cobalamin is an important cofactor for many enzymes, such as methyltransferases, isomerases or reductases [74]. Besides, affecting cobalamin synthesis may in turn impact for example chlorophyll synthesis by depriving Mg-protoporphyrin IX-monomethylester oxidative cyclase (Q2RNF3) of its cofactor even if we did not observe any change at the proteins level [75]. Cobalamin is also important for the S-adenosyl methionine (SAM) regeneration necessary for the various enzymes relying on it for substrate methylation, as indeed one of the two existing pathways relies on a cobalamin dependent methionine synthase (Q2RU64 in *R. rubrum*) [76]. Furthermore, hydrogenobyrinic acid synthase (CobZ) necessary for cobalamin synthesis is an enzyme containing heme, Flavin and Fe-S cofactors [77]. These few examples highlight the high interdependency of these cofactors biosynthesis (See **Figure 6**).

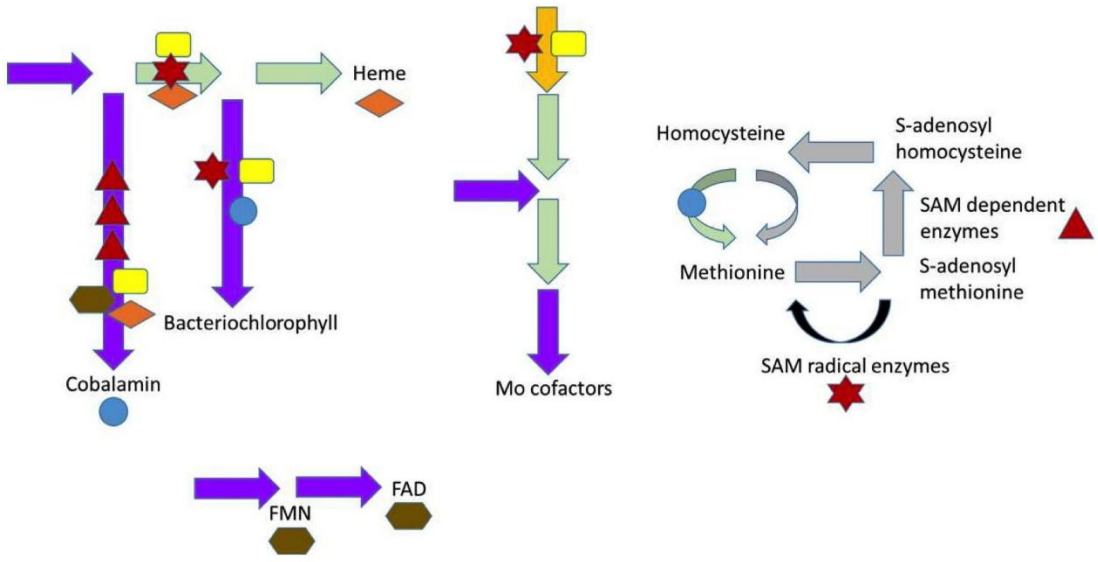

Figure 6: cofactors biosynthesis interdependency.

This figure is a scheme of the interdependency between various cofactor biosynthesis and is not intended to be exhaustive. Arrows represent branches of the different pathways with grey arrows: no proteins detected; green arrows: the proteins detected are invariants; orange and purple arrows: at least one of the detected proteins are up- or down-regulated respectively (See **Supplementary Figures 7, 8** and **Figure 7** below for more details). Yellow squares: iron-sulfur clusters; brown hexagons: flavins; blue circles: cobalamin; orange diamonds: hemes; red stars and triangles: SAM (S-adenosyl methionine) in the context of SAM radical and SAM dependent (methyl transferase) enzymes.Note that colored forms indicate the presence and not the number of

these cofactors; the three red triangles in cobalamin synthesis are just there to highlight an important number of such proteins.

It is worth mentioning that cobalamin is also implicated directly or indirectly, in gene expression regulation. Indeed, in several photosynthetic bacteria, RNA-based Co-riboswitches regulate the synthesis of proteins implicated for example in cobalamin or carotenoids synthesis [78]. Several riboswitches respond to the different forms of cobalamin (methylcobalamin and adenosylcobalamin) as well as to their photolytic derivative (hydroxocobalamin) [79]. Moreover, in some photosynthetic bacteria like *Rhodobacter capsulatus,* AerR when it binds cobalamin, acts as an anti-repressor of CrtJ preventing the binding of this transcription repressor to various promotors [80]. A decrease in cobalamin synthesis could therefore result in the perturbation of various proteins transcriptional regulation.

Riboflavin metabolism

Concerning riboflavin metabolism, all the enzymes from GTP to FMN and FAD are moderately down-regulated (fold-change between 0.48 and 0.86) (**Supplementary Figure 8**). Note that the enzyme corresponding to EC. 3.1.3.104 has not yet been identified in *R. rubrum*. Many redox enzymes use FAD or FMN and may therefore be affected by such an inhibition in term of regulation, stability or merely function. In particular, one can cite the previously mentioned flavoprotein CobZ implicated in cobalamin biosynthesis (**Figure 6**).

Molybdopterin cofactor biosynthesis

Concerning the molybdopterin cofactor (Moco) biosynthesis and its derivatives, proteins homologous to most of the ones described by Leimkühler *et al.* or Zupok *et al.* for *Escherichia coli* are annotated in *R. rubrum* [81, 82]. In the pathway, MoaB (Q2RXS2), MoaD (Q2RQI4), MoaE (Q2RQI3), MoeA (Q2RS73) are invariant, and MobB (Q2RSN8) and MoeB (Q2RMQ8) slightly down-regulated (**Figure 7**). The role of MobB is not very clear but MoeB participates with IscS to the regeneration of the thiocarboxylate group on MoaD which itself is essential in association with MoaE to form the dithiolated molybdopterin intermediate [82]. The organization of the corresponding genes on *R. rubrum* chromosome is quite different from the one in *E. coli*, and even from the one in *R. capsulatus* which is phylogenetically closer (alphaproteobacteria) [83]. Except for a cluster MobAMoaCDE, other proteins implicated in molybdopterin cofactor biosynthesis are individually located.

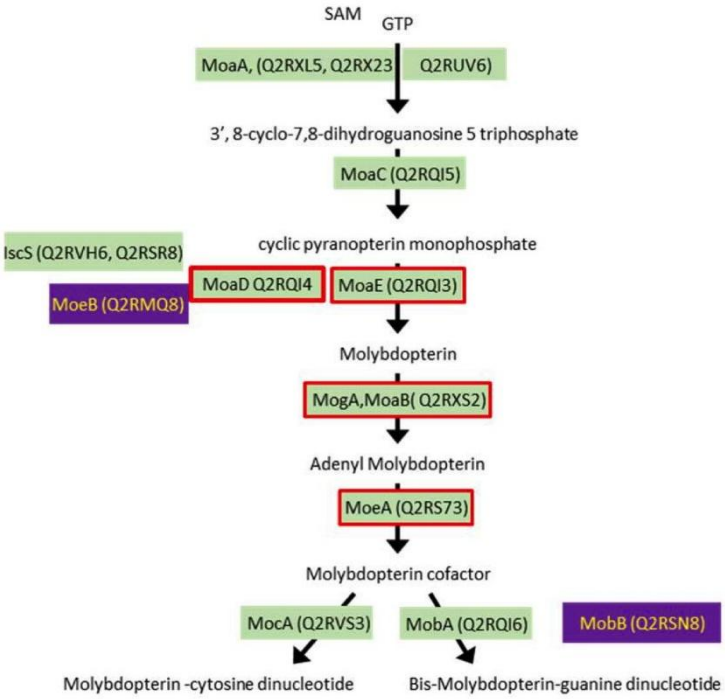

Figure 7: Molybdenum cofactors biosynthesis
This figure was made based on KEGG mapper (https://www.genome.jp/kegg/mapper.html) rru00790 Folate biosynthesis with modifications according to Leimkuhler S and Zupok A [81, 82]. Green rectangles represent enzymatic functions to which KEGG program has associated at least one protein from *R. rubrum*; the red borders around the green rectangles indicate that these proteins were identified in our proteome (2D and shotgun approaches). Purple and orange rectangles indicate down- and up-regulated proteins with their uniprot reference.

The proteins encoded by the cluster around *moeB* are interesting. Q2RMQ6 is a transcriptional regulator belonging to the BadM/Rrf2 family; Q2RMQ7 is a cysteine synthase and Q2RMQ9 is a hypothetical protein but contains an IPR027396 DsrEFH-like and IPR003787 Sulphur_relay_DrsE/F-like domain. DsrE is a small soluble protein involved in intracellular sulfur trafficking and delivery to the sulfite reductase which is a molybdoenzyme [84]. Q2RMQ6 and Q2RMQ8 are down regulated (0.8 and 0.5 folds, respectively), Q2RMQ7 invariant and Q2RMQ9 not detected.
Rru_A1287 is predicted to code for a trimethylamine-N-oxide reductase/Dimethylsulfoxide reductase (cytochrome c) (Q2RUV7, TMAO/DMSO reductase, TorA), Rru_A1284 for the cytoplasmic chaperone TorD (Q2RUW0), Rru_A1283 for a membrane-bound tetraheme cytochrome TorC (Q2RUW1) and Rru_A1282 for the two component transcriptional regulator TorR (Q2RUW2). Whereas Q2RUV7 (TMAO reductase) protein was down-regulated and Q2RUW1 (TorC) protein invariant, TorD (Q2RUW0) chaperone which is essential for molybdopterin insertion in the dimethyl sulfoxide reductase family was up-regulated [85]. This suggests that even if the molybdoprotein is down-regulated, its maturation machinery properly seems stimulated. Another moaA protein (Q2RXL5, not detected in our study) is next to the molybdo-protein formate dehydrogenase.
We therefore decided to look more precisely at molybdopterin binding proteins as, in some cases, a lack of their cofactor may alter their stability or modify their regulation. Several of them varied in abundance. However, it is difficult with *R. rubrum* to be sure of their "identity" as the genome annotations are mainly automatic and the experimental data very scarce.
Q2RVS8 which is down regulated (0.4 folds) in our conditions after CO exposure, could correspond to a Xanthine dehydrogenase, molybdenum binding subunit or rather to an aerobic carbon-monoxide dehydrogenase large subunit found in some carboxydotrophic bacteria. Aerobic CODHs are members of the Xanthine oxidoreductase family and catalyze the oxidation of CO to CO_2 under aerobic

conditions using a quinone as electron acceptor. This enzyme complex is composed of three subunits and contains a FAD, two [2Fe-2S] clusters as well as a binuclear Mo-Cu active site. Using the well-characterized three subunits of the enzyme from *Oligotropha carboxidovorans* for Blast analyses against *R. rubrum*, we could indeed identified the three contiguous proteins Q2RVS7 (FAD binding subunit), Q2RVS8 (molybdenum binding subunit), and Q2RVS9 (Iron-sulfur binding subunit) (See **Supplementary Figure 9**). However, Q2RVS7 and Q2RVS9 are invariant and not detected, respectively. Unexpectedly, an aerobic CODH is probably present in *R. rubrum*, even under anaerobic conditions.
Q2RXM7 the gene of which is located in the formate hydrogenlyase cluster (**Figure 4**) is annotated as aldehyde ferredoxin oxidoreductase and is highly induced (9 folds).
In the same cluster, the formate dehydrogenase alpha subunit (Q2RXL6) which is part of the formate hydrogenlyase complex, is slightly down-regulated (0.73 folds) and this protein is known to be CO sensitive.
Molybdo-proteins are relatively scarce in proteomes (around 14-19 in *E. coli* for example) [86]. In *R. rubrum*, based on sequences, we identified 9 potential molybdopterin cofactor binding proteins, one not detected in our proteome and the eight remaining ones up or down regulated. Even if their function is unclear, we can pinpoint that this class of protein is over represented among varying proteins. These variations could be directly associated with the defect in Moco biosynthesis that could for example decrease protein stability or be a regulation of the apoprotein synthesis. Indeed, as for cobalamin, FMN and SAM, it exists riboswitches fixing molybdenum cofactor (Moco-riboswitches) that are often located upstream of genes encoding molybdate transporters, molybdenum cofactor biosynthesis enzymes, and even proteins that use Moco as a coenzyme [87]. Besides Rosenthel and colleagues showed that molyddate itself up-regulates *E. coli* hydrogenase-3 and formate dehydrogenase, and repress the transcription of modABC operon [88]. In our case, we have less formate dehydrogenase and ModA is up-regulated like if there was less molybdenum at least bio-available in the cells after CO exposure.

Iron-sulfur clusters
Iron-sulfur clusters form an important category of cofactors, playing central roles in the cell as prosthetic groups for electron transfer in many key proteins or even implicated in transcriptional regulation and sensing. Three types of iron-sulfur cluster biogenesis machinery have been described in the literature: the primary system ISC, typically found in bacteria and eukaryotes, the NIF machinery found in nitrogen-fixing organisms and the SUF machinery. The SUF system is similar to the ISC one but is described as operative under stress conditions (iron starvation or oxidative stress) in some bacteria such as *E. coli*. However, the SUF system is also described as the sole iron-sulfur cluster biogenesis system in archaea, cyanobacteria and some gram-positive bacteria [89]. The SUF system is composed of the SufBCD complex onto which iron-sulfur clusters are transiently assembled and the two-component cysteine desulfurase complex, SufSE, which mobilizes sulfur from L-cysteine. Finally, the carrier SufA delivers Fe–S clusters to target apo-proteins [90]. In *R. rubrum*, the *suf* locus *sufRBCDSEA* is present. The cysteine desulfurase SufS is up-regulated in our study (Q2RR78, 1.4 folds). This tends to indicate that upon CO exposure, the bacterium needs to use cysteine to generate elemental sulfur usable for new iron-sulfur clusters. This hypothesis is also supported by the fact that two other proteins in the *suf* operon are also up-regulated (Q2RR75, sufB 1.15 folds and Q2RR76, sufC 1.8 folds), even if, SufD (Q2RR77) is invariant.
Q2RNH0, annotated as a Nitrogen-fixing NifU-like protein is up-regulated in shotgun but down-regulated in 2D-gel approach suggesting that the protein is regulated both in term of total amount as detected by the shotgun experiment and by post-translational modifications (note that one or several up-regulated spots of the protein are probably missed on the 2D-gel). However, the protein shows some strong homologies with NfuA with the C151XXC154 signature motif for the binding of an intermolecular 4Fe4S cluster. NfuA is a protein involved in iron-sulfur cluster biogenesis under severe conditions and is up-regulated via IscR under conditions of iron depletion or oxidative stress in *E. coli* [91]. NfuA can transfer its [4Fe-4S] cluster to apoproteins, and thereby intervenes in the maturation of

Fe/S proteins or act as a scaffold/chaperone for damaged Fe/S proteins. The gene upstream of the one coding for Q2RNH0 encodes a protein similar to UspA (Universal stress protein, Q2RS59) the induction of which occurs in *E. coli* whenever conditions cause for example growth arrest. The protein is also up-regulated in our study after CO exposure.

3.5. Comparison with other studies

As mentioned in the introduction, several OMICS studies have already been performed to study CO metabolism in carboxydotrophs or the potential of CO as a bactericidal agent in the model bacterium *E. coli* for example.

Carboxydotrophic microorganisms are able to use CO as energy and/or carbon source and produce methane (methanogens), acetate (acetogens) or hydrogen (hydrogenogens), or to reduce sulfate (sulfate-reducers). Diender *et al.* performed a proteomic analysis on the methanogen *Methanothermobacter marburgensis* which highlighted a higher abundance of proteins involved in redox metabolism when cells were grown in H_2/CO_2 plus CO, including the universal stress protein (usp) also found up-regulated in our study [92]. Curiously, many of these proteins are rather known to respond to oxidative stress whereas CO is a strong reductant. Rajeev *et al.* performed a transcriptomic analysis on *Desulfovibrio vulgaris* [93]. The study showed that CO differentially alters the expression of many genes coding for proteins implicated in electron transfer activities. However, although *D. vulgaris* is able to grow but very slowly with CO as a sole source of energy this gas is toxic to this bacterium as it is for most other sulfate-reducing bacteria [94]. Moon *et al.* performed a proteomic study on the hydrogenogenic archaeon *Thermococcus onnurineus NA1* to analyze its metabolism on different carbon source (CO, formate, starch) [95]. They showed that in CO condition, some stress response proteins like alkyl hydroperoxide reductase, thioredoxin peroxidase, NAD(P)H:rubredoxin oxidoreductase and rubrerythrin were induced. Besides, the Moco synthesis is also down-regulated and iron transport altered. More recently, Fukuyama *et al.* performed a whole transcriptome analysis on another hydrogenogenic carboxydotroph: *Carboxydothermus pertinax* [96]. The data show that *C. pertinax* switches its metabolism by altering massively the expression of a low number of gene clusters including ferrous iron transport (23).

Due to the low solubility of CO in aqueous solutions, its intracellular concentration is usually not sufficient to exert an antimicrobial action. Molecules releasing CO directly inside the bacteria (or the cells) have therefore been developed (CO releasing molecules, CORM) [97].

Many OMICS studies have been performed in particular on *E. coli* to better understand CORM toxicity, knowing that in plus of CO these molecules contains a metallic atom (often Ru) that can also contribute to the observed toxicity [98]. For example, the transcriptomic study of Davidge *et al.* showed that key aerobic respiratory complexes are affected which is rather expected as heme is a well-known binding site for CO [99]. However, the transcription of several genes encoding proteins associated with metal metabolism, transport and homeostasis, are also affected. Their transcriptomic data probabilistic analysis hinted at several global transcriptomic regulator including Fis (Factor-for-inversion stimulation protein), FNR, Fur and Cpx. Several members of these regulator families are also modified at the protein level in our study. Wareham *et al.* showed that the response of *E. coli* to CO is global with regulation of more than 20% of the genome (central energy metabolism, amino acid synthesis and in particular sulfur amino acid, and iron acquisition via the implication of ArcA (Aerobic respiration control protein), FNR or PdhR (pyruvate dehydrogenase)) [97]. They observed important variations between aerobic and anaerobic cultures. With CORM, free iron pool is depleted and more siderophores are excreted. The bacteria respond as if CO induced a transition to a more anoxic-like state. As another example, the study of Wilson *et al* clearly showed by transcriptomic that CO release mainly affects iron acquisition and utilization, zinc homeostasis and global stress responses, and this even in a heme-deleted *E. coli* mutant [17]. Most of the iron systems up-regulated in their study are also affected in the same way in *R. rubrum* (fecI, fep ou fhu, tonB). Except tonB, these proteins are supposed not to be regulated by Fur in *E. coli*. Even if heme is an important target of CO, this study clearly showed that it is not the only one. In 2019, Carvalho *et al.* made a metabolomic study on *E. coli* exposed to CORM-3 molecule. They showed that the toxicity resulted in particular from the inhibition

of the glutamate synthase and two enzymes of the TCA cycle (aconitase, and fumarase) which are all bearing iron-sulfur clusters, with a labile position (note that *Escherichia coli* contains three distinct fumarases one of which does not contain an iron-sulfur cluster). The authors suggest that CO targets their metallic centers. They also showed that CO triggers a perturbation in redox homeostasis.
We can notice that in many respect, our results highlighted a response of *R. rubrum* similar to that of *E. coli* after exposure to CO or CORM molecules. Our experimental conditions have forced this response as we intentionally exposed *R. rubrum* to a high CO concentration (100% CO, almost 1 atm of overpressure). *R. rubrum* can grow, in the dark even with 100% CO in the headspace but the doubling time is inversely related to CO concentration [29]. *R. rubrum* ECH is highly CO tolerant but nonetheless in crude membrane, inhibition starts to appear above 60% CO in the headspace [100]. We can notice that out of the five enzymes described by Revelles *et al.*, as involved in CO_2 fixation with syngas in *R. rubrum*, two are invariant (Q2RQS7, 2-oxoglutarate synthase and Q53046, Pyruvate-flavodoxin oxidoreductase (PFOR)), and one is down-regulated (Q2RSU7, 5-methylthioribulose-1-phosphate isomerase) (**Figure 2**) [3]. This strongly suggests that in our conditions, *R. rubrum* has not increased its CO/CO_2 assimilation capacity in response to CO addition, at least at the time of the sampling. Moreover, as described above, the "toxic" effect observed for *R. rubrum* is also visible at least partially with other carboxydotrophs (metal homeostasis perturbation and triggering of stress response proteins) suggesting that all these organisms even if able to use CO for growth cannot avoid part of the toxic effect of CO.

4. Conclusions

In conclusion, carboxydotrophs, and in particular *R. rubrum*, seem to have evolved specific enzymes like CODH and some enzymes more resistant to CO such as ECH hydrogenase, in order to convert the CO and recover the energy resulting from this reaction. *R. rubrum* has also evolved systems to protect some of its enzymes like the CowN protein that prevents damage to the nitrogenase in the presence of CO [101].
However, even if the CODH itself plays a role in CO detoxification, our study clearly shows that metal homeostasis and metallic cofactor are affected in particular concerning Fe, Co, and Mo. One could also expect proteins dealing with Ni to change; however, a high concentration of 50 µM of Ni was used in the medium. Increasing metal concentration in the culture medium could therefore be beneficial and adding synthesis intermediates like vitamin B12 for example, might also help if the bacterium possesses an appropriate uptake system. It is also worth noting that CODH, CooF, and ECH that are strongly CO-induced contain many iron-sulfur clusters, and may contribute to deplete or at least decrease the iron and sulfur pools, which could explain the up-regulation of the suf operon.
Moreover, as summarize in **Figure 6**, the syntheses of several cofactors are interdependent and a defect in one pathway may end-up affecting all of them. Studies at the molecular level would be interesting to understand the precise effect of CO binding. For example, it is often claimed that CO affects iron-sulfur clusters but unlike NO, there is a lack of experimental data. It would be of great interest to study more precisely at the molecular level whether transcription regulators such as Fur are directly disturbed by the binding of CO. As well, the perturbation in molybdenum cofactor biosynthesis could be linked either to a direct interaction of CO with Mo or just to a defect of one enzyme in its biosynthesis pathways. Addressing these issues would be the next step in the understanding of CO toxicity that may decrease the efficiency of biological WGSR, or CH_4 or PHB production by carboxydotrophs.

Data Availability

The shotgun mass spectrometry data have been deposited to the ProteomeXchange Consortium via the PRIDE partner repository with the dataset identifier PXD025489 and 10.6019/PXD025489 [108]. The mass spectrometry datasets generated during the 2-D gel approach are available from the corresponding authors on reasonable request.

References

[1] L. Hendrickx, H. De Wever, V. Hermans, F. Mastroleo, N. Morin, A. Wilmotte, P. Janssen, M. Mergeay, Microbial ecology of the closed artificial ecosystem MELiSSA (Micro-Ecological Life Support System Alternative): reinventing and compartmentalizing the Earth's food and oxygen regeneration system for long-haul space exploration missions, Res Microbiol, 157(1) (2006), p. 77-86.

[2] D. Bonam, S.A. Murrell, P.W. Ludden, Carbon monoxide dehydrogenase from Rhodospirillum rubrum, J Bacteriol, 159(2) (1984), p. 693-9.

[3] O. Revelles, N. Tarazona, J.L. Garcia, M.A. Prieto, Carbon roadmap from syngas to polyhydroxyalkanoates in Rhodospirillum rubrum, Environ Microbiol, 18(2) (2016), p. 708-20.

[4] B. Leroy, Q. De Meur, C. Moulin, G. Wegria, R. Wattiez, New insight into the photoheterotrophic growth of the isocytrate lyase-lacking purple bacterium Rhodospirillum rubrum on acetate, Microbiology, 161(Pt 5) (2015), p. 1061-1072.

[5] M. Alfano, C. Cavazza, The biologically mediated water-gas shift reaction: structure, function and biosynthesis of monofunctional [NiFe]-carbon monoxide dehydrogenases, Sustain Energ Fuels, 2(8) (2018), p. 1653-1670.

[6] M. Alfano, J. Perard, R. Miras, P. Catty, C. Cavazza, Biophysical and structural characterization of the putative nickel chaperone CooT from Carboxydothermus hydrogenoformans, J Biol Inorg Chem, 23(5) (2018), p. 809-817.

[7] M. Alfano, J. Perard, P. Carpentier, C. Basset, B. Zambelli, J. Timm, S. Crouzy, S. Ciurli, C. Cavazza, The carbon monoxide dehydrogenase accessory protein CooJ is a histidine-rich multidomain dimer containing an unexpected Ni(II)-binding site, Journal of Biological Chemistry, 294(19) (2019), p. 7601-7614.

[8] G. Wang, Y. Gong, Q. Zhang, M. Zhou, Formation and characterization of magnesium bisozonide and carbonyl complexes in solid argon, J Phys Chem A, 114(40) (2010), p. 10803-9.

[9] K. Seufert, M.L. Bocquet, W. Auwarter, A. Weber-Bargioni, J. Reichert, N. Lorente, J.V. Barth, Cis-dicarbonyl binding at cobalt and iron porphyrins with saddle-shape conformation, Nat Chem, 3(2) (2011), p. 114-9.

[10] H.R. Lucas, K.D. Karlin, Copper-Carbon Bonds in Mechanistic and Structural Probing of Proteins as well as in Situations where Copper is a Catalytic or Receptor Site, Met Ions Life Sci, 6 (2009), p. 295-361.

[11] D.H. Flint, R.M. Allen, Iron-Sulfur Proteins with Nonredox Functions, Chem Rev, 96(7) (1996), p. 2315-2334.

[12] M.A. Vanoni, B. Curti, Structure--function studies on the iron-sulfur flavoenzyme glutamate synthase: an unexpectedly complex self-regulated enzyme, Arch Biochem Biophys, 433(1) (2005), p. 193-211.

[13] C.H. Arnett, M.J. Chalkley, T. Agapie, A Thermodynamic Model for Redox-Dependent Binding of Carbon Monoxide at Site-Differentiated, High Spin Iron Clusters, J Am Chem Soc, 140(16) (2018), p. 5569-5578.

[14] M.E. Pandelia, H. Ogata, L.J. Currell, M. Flores, W. Lubitz, Inhibition of the [NiFe] hydrogenase from Desulfovibrio vulgaris Miyazaki F by carbon monoxide: an FTIR and EPR spectroscopic study, Biochim Biophys Acta, 1797(2) (2010), p. 304-13.

[15] B.J. Lemon, J.W. Peters, Binding of exogenously added carbon monoxide at the active site of the iron-only hydrogenase (CpI) from Clostridium pasteurianum, Biochemistry, 38(40) (1999), p. 12969-73.

[16] L.K. Wareham, R.K. Poole, M. Tinajero-Trejo, CO-releasing Metal Carbonyl Compounds as Antimicrobial Agents in the Post-antibiotic Era, Journal of Biological Chemistry, 290(31) (2015), p. 18999-19007.

[17] J.L. Wilson, L.K. Wareham, S. McLean, R. Begg, S. Greaves, B.E. Mann, G. Sanguinetti, R.K. Poole, CO-Releasing Molecules Have Nonheme Targets in Bacteria: Transcriptomic, Mathematical Modeling and Biochemical Analyses of CORM-3 [Ru(CO)(3)Cl(glycinate)] Actions on a Heme-Deficient Mutant of Escherichia coli, Antioxid Redox Sign, 23(2) (2015), p. 148-162.

[18] S.M. Carvalho, J. Marques, C.C. Romao, L.M. Saraiva, Metabolomics of Escherichia coli Treated with the Antimicrobial Carbon Monoxide-Releasing Molecule CORM-3 Reveals Tricarboxylic Acid Cycle as Major Target, Antimicrob Agents Chemother, 63(10) (2019).

[19] D. Stucki, W. Stahl, Carbon monoxide - beyond toxicity?, Toxicol Lett (2020).

[20] R.N. Watts, P. Ponka, D.R. Richardson, Effects of nitrogen monoxide and carbon monoxide on molecular and cellular iron metabolism: mirror-image effector molecules that target iron, Biochem J, 369(Pt 3) (2003), p. 429-40.

[21] D.W. Reif, R.D. Simmons, Nitric oxide mediates iron release from ferritin, Arch Biochem Biophys, 283(2) (1990), p. 537-41.

[22] S. Nader, J. Perard, P. Carpentier, L. Arnaud, S. Crouzy, I. Michaud-Soret, New insights into the tetrameric family of the Fur metalloregulators, Biometals, 32(3) (2019), p. 501-519.
[23] B.E. Ahn, J. Cha, E.J. Lee, A.R. Han, C.J. Thompson, J.H. Roe, Nur, a nickel-responsive regulator of the Fur family, regulates superoxide dismutases and nickel transport in Streptomyces coelicolor, Mol Microbiol, 59(6) (2006), p. 1848-58.
[24] R.L. Kerby, H. Youn, G.P. Roberts, RcoM: a new single-component transcriptional regulator of CO metabolism in bacteria, J Bacteriol, 190(9) (2008), p. 3336-43.
[25] A. Mikhaylina, A.Z. Ksibe, D.J. Scanlan, C.A. Blindauer, Bacterial zinc uptake regulator proteins and their regulons, Biochem Soc Trans, 46(4) (2018), p. 983-1001.
[26] J. Green, M.S. Paget, Bacterial redox sensors, Nat Rev Microbiol, 2(12) (2004), p. 954-66.
[27] K. Hantke, Iron and metal regulation in bacteria, Curr Opin Microbiol, 4(2) (2001), p. 172-7.
[28] W.B. Jeon, S.W. Singer, P.W. Ludden, L.M. Rubio, New insights into the mechanism of nickel insertion into carbon monoxide dehydrogenase: analysis of Rhodospirillum rubrum carbon monoxide dehydrogenase variants with substituted ligands to the [Fe3S4] portion of the active-site C-cluster, J Biol Inorg Chem, 10(8) (2005), p. 903-12.
[29] R.L. Kerby, P.W. Ludden, G.P. Roberts, Carbon Monoxide-Dependent Growth of Rhodospirillum-Rubrum, Journal of Bacteriology, 177(8) (1995), p. 2241-2244.
[30] S. Luche, V. Santoni, T. Rabilloud, Evaluation of nonionic and zwitterionic detergents as membrane protein solubilizers in two-dimensional electrophoresis, Proteomics, 3(3) (2003), p. 249-53.
[31] T. Rabilloud, Optimization of the cydex blue assay: A one-step colorimetric protein assay using cyclodextrins and compatible with detergents and reducers, PLoS One, 13(4) (2018), p. e0195755.
[32] L. Muller, L. Fornecker, M. Chion, A. Van Dorsselaer, S. Cianferani, T. Rabilloud, C. Carapito, Extended investigation of tube-gel sample preparation: a versatile and simple choice for high throughput quantitative proteomics, Sci Rep, 8(1) (2018), p. 8260.
[33] T. Lyubimova, S. Caglio, C. Gelfi, P.G. Righetti, T. Rabilloud, Photopolymerization of polyacrylamide gels with methylene blue, Electrophoresis, 14(1-2) (1993), p. 40-50.
[34] R. Prudent, N. Demoncheaux, H. Diemer, V. Collin-Faure, R. Kapur, F. Paublant, L. Lafanechere, S. Cianferani, T. Rabilloud, A quantitative proteomic analysis of cofilin phosphorylation in myeloid cells and its modulation using the LIM kinase inhibitor Pyr1, PLoS One, 13(12) (2018), p. e0208979.
[35] C. Tastet, P. Lescuyer, H. Diemer, S. Luche, A. van Dorsselaer, T. Rabilloud, A versatile electrophoresis system for the analysis of high- and low-molecular-weight proteins, Electrophoresis, 24(11) (2003), p. 1787-94.
[36] B. Dalzon, J. Bons, H. Diemer, V. Collin-Faure, C. Marie-Desvergne, M. Dubosson, S. Cianferani, C. Carapito, T. Rabilloud, A Proteomic View of Cellular Responses to Anticancer Quinoline-Copper Complexes, Proteomes, 7(2) (2019).
[37] A.G. Herrmann, J.L. Searcy, T. Le Bihan, J. McCulloch, R.F. Deighton, Total variance should drive data handling strategies in third generation proteomic studies, Proteomics, 13(22) (2013), p. 3251-5.
[38] M. Kanehisa, Y. Sato, KEGG Mapper for inferring cellular functions from protein sequences, Protein Sci, 29(1) (2020), p. 28-35.
[39] F. Mastroleo, B. Leroy, R. Van Houdt, C. s' Heeren, M. Mergeay, L. Hendrickx, R. Wattiez, Shotgun proteome analysis of Rhodospirillum rubrum S1H: integrating data from gel-free and gel-based peptides fractionation methods, J Proteome Res, 8(5) (2009), p. 2530-41.
[40] G. Bayon-Vicente, R. Wattiez, B. Leroy, Global Proteomic Analysis Reveals High Light Intensity Adaptation Strategies and Polyhydroxyalkanoate Production in Rhodospirillum rubrum Cultivated With Acetate as Carbon Source, Front Microbiol, 11 (2020), p. 464.
[41] R.A. Verlinden, D.J. Hill, M.A. Kenward, C.D. Williams, I. Radecka, Bacterial synthesis of biodegradable polyhydroxyalkanoates, J Appl Microbiol, 102(6) (2007), p. 1437-49.
[42] T. Narancic, E. Scollica, G. Cagney, K.E. O'Connor, Three novel proteins co-localise with polyhydroxybutyrate (PHB) granules in Rhodospirillum rubrum S1, Microbiology, 164(4) (2018), p. 625-634.
[43] R. Handrick, S. Reinhardt, D. Schultheiss, T. Reichart, D. Schuler, V. Jendrossek, D. Jendrossek, Unraveling the function of the Rhodospirillum rubrum activator of polyhydroxybutyrate (PHB) degradation: the activator is a PHB-granule-bound protein (phasin), J Bacteriol, 186(8) (2004), p. 2466-75.
[44] R. Handrick, S. Reinhardt, P. Kimmig, D. Jendrossek, The "intracellular" poly(3-hydroxybutyrate) (PHB) depolymerase of Rhodospirillum rubrum is a periplasm-located protein with specificity for native PHB and with structural similarity to extracellular PHB depolymerases, J Bacteriol, 186(21) (2004), p. 7243-53.
[45] S. Tripathi, T.L. Poulos, Testing the N-Terminal Velcro Model of CooA Carbon Monoxide Activation, Biochemistry, 57(21) (2018), p. 3059-3064.

[46] L. Forzi, R.G. Sawers, Maturation of [NiFe]-hydrogenases in Escherichia coli, Biometals, 20(3-4) (2007), p. 565-78.
[47] J. Schiffels, O. Pinkenburg, M. Schelden, H.A. Aboulnaga el, M.E. Baumann, T. Selmer, An innovative cloning platform enables large-scale production and maturation of an oxygen-tolerant [NiFe]-hydrogenase from Cupriavidus necator in Escherichia coli, PLoS One, 8(7) (2013), p. e68812.
[48] A.J. Finney, G. Buchanan, T. Palmer, S.J. Coulthurst, F. Sargent, Activation of a [NiFe]-hydrogenase-4 isoenzyme by maturation proteases, Microbiology (Reading), 166(9) (2020), p. 854-60.
[49] K. Wawrousek, S. Noble, J. Korlach, J. Chen, C. Eckert, J. Yu, P.C. Maness, Genome annotation provides insight into carbon monoxide and hydrogen metabolism in Rubrivivax gelatinosus, PLoS One, 9(12) (2014), p. e114551.
[50] J.D. Fox, Y. He, D. Shelver, G.P. Roberts, P.W. Ludden, Characterization of the region encoding the CO-induced hydrogenase of Rhodospirillum rubrum, J Bacteriol, 178(21) (1996), p. 6200-8.
[51] Y. He, D. Shelver, R.L. Kerby, G.P. Roberts, Characterization of a CO-responsive transcriptional activator from Rhodospirillum rubrum, J Biol Chem, 271(1) (1996), p. 120-3.
[52] P.M. Vignais, B. Toussaint, Molecular biology of membrane-bound H2 uptake hydrogenases, Arch Microbiol, 161(1) (1994), p. 1-10.
[53] M. Kammler, C. Schon, K. Hantke, Characterization of the ferrous iron uptake system of Escherichia coli, J Bacteriol, 175(19) (1993), p. 6212-9.
[54] C.K. Lau, H. Ishida, Z. Liu, H.J. Vogel, Solution structure of Escherichia coli FeoA and its potential role in bacterial ferrous iron transport, J Bacteriol, 195(1) (2013), p. 46-55.
[55] N. Cadieux, C. Bradbeer, E. Reeger-Schneider, W. Koster, A.K. Mohanty, M.C. Wiener, R.J. Kadner, Identification of the periplasmic cobalamin-binding protein BtuF of Escherichia coli, J Bacteriol, 184(3) (2002), p. 706-17.
[56] M.M. Gibson, D.A. Bagga, C.G. Miller, M.E. Maguire, Magnesium transport in Salmonella typhimurium: the influence of new mutations conferring Co2+ resistance on the CorA Mg2+ transport system, Mol Microbiol, 5(11) (1991), p. 2753-62.
[57] N. Zhang, X. Ren, D. Zhu, D. Li, D. Wang, Crystallization and preliminary crystallographic studies of CorC, a magnesium-ion transporter, Acta Crystallogr Sect F Struct Biol Cryst Commun, 66(Pt 6) (2010), p. 681-3.
[58] P. Gimenez-Mascarell, I. Gonzalez-Recio, C. Fernandez-Rodriguez, I. Oyenarte, D. Muller, M.L. Martinez-Chantar, L.A. Martinez-Cruz, Current Structural Knowledge on the CNNM Family of Magnesium Transport Mediators, Int J Mol Sci, 20(5) (2019).
[59] S.Z. Wang, Y. Chen, Z.H. Sun, Q. Zhou, S.F. Sui, Escherichia coli CorA periplasmic domain functions as a homotetramer to bind substrate, Journal of Biological Chemistry, 281(37) (2006), p. 26813-26820.
[60] R.K. Watt, P.W. Ludden, Ni(2+) transport and accumulation in Rhodospirillum rubrum, J Bacteriol, 181(15) (1999), p. 4554-60.
[61] M.F. Fillat, The FUR (ferric uptake regulator) superfamily: diversity and versatility of key transcriptional regulators, Arch Biochem Biophys, 546 (2014), p. 41-52.
[62] E. Pohl, J.C. Haller, A. Mijovilovich, W. Meyer-Klaucke, E. Garman, M.L. Vasil, Architecture of a protein central to iron homeostasis: crystal structure and spectroscopic analysis of the ferric uptake regulator, Mol Microbiol, 47(4) (2003), p. 903-15.
[63] M.A. Sheikh, G.L. Taylor, Crystal structure of the Vibrio cholerae ferric uptake regulator (Fur) reveals insights into metal co-ordination, Mol Microbiol, 72(5) (2009), p. 1208-20.
[64] B.A. Gilston, S. Wang, M.D. Marcus, M.A. Canalizo-Hernandez, E.P. Swindell, Y. Xue, A. Mondragon, T.V. O'Halloran, Structural and mechanistic basis of zinc regulation across the E. coli Zur regulon, PLoS Biol, 12(11) (2014), p. e1001987.
[65] D. Lucarelli, S. Russo, E. Garman, A. Milano, W. Meyer-Klaucke, E. Pohl, Crystal structure and function of the zinc uptake regulator FurB from Mycobacterium tuberculosis, J Biol Chem, 282(13) (2007), p. 9914-22.
[66] M. Kebouchi, F. Saul, R. Taher, A. Landier, B. Beaudeau, S. Dubrac, P. Weber, A. Haouz, M. Picardeau, N. Benaroudj, Structure and function of the Leptospira interrogans peroxide stress regulator (PerR), an atypical PerR devoid of a structural metal-binding site, J Biol Chem, 293(2) (2018), p. 497-509.
[67] G.F. White, C. Singleton, J.D. Todd, M.R. Cheesman, A.W. Johnston, N.E. Le Brun, Heme binding to the second, lower-affinity site of the global iron regulator Irr from Rhizobium leguminosarum promotes oligomerization, FEBS J, 278(12) (2011), p. 2011-21.
[68] A.W. Johnston, J.D. Todd, A.R. Curson, S. Lei, N. Nikolaidou-Katsaridou, M.S. Gelfand, D.A. Rodionov, Living without Fur: the subtlety and complexity of iron-responsive gene regulation in the symbiotic bacterium Rhizobium and other alpha-proteobacteria, Biometals, 20(3-4) (2007), p. 501-11.

[69] D.A. Rodionov, M.S. Gelfand, J.D. Todd, A.R. Curson, A.W. Johnston, Computational reconstruction of iron- and manganese-responsive transcriptional networks in alpha-proteobacteria, PLoS Comput Biol, 2(12) (2006), p. e163.
[70] D. Nam, Y. Matsumoto, T. Uchida, M.R. O'Brian, K. Ishimori, Mechanistic insights into heme-mediated transcriptional regulation via a bacterial manganese-binding iron regulator, iron response regulator (Irr), J Biol Chem, 295(32) (2020), p. 11316-11325.
[71] C. Singleton, G.F. White, J.D. Todd, S.J. Marritt, M.R. Cheesman, A.W. Johnston, N.E. Le Brun, Heme-responsive DNA binding by the global iron regulator Irr from Rhizobium leguminosarum, J Biol Chem, 285(21) (2010), p. 16023-31.
[72] H. Fang, J. Kang, D. Zhang, Microbial production of vitamin B12: a review and future perspectives, Microb Cell Fact, 16(1) (2017), p. 15.
[73] R. Ghosh, E. Roth, K. Abou-Aisha, R. Saegesser, C. Autenrieth, The monofunctional cobalamin biosynthesis enzyme precorrin-3B synthase (CobZRR) is essential for anaerobic photosynthesis in Rhodospirillum rubrum but not for aerobic dark metabolism, Microbiology, 164(11) (2018), p. 1416-1431.
[74] K. Gruber, B. Puffer, B. Krautler, Vitamin B12-derivatives-enzyme cofactors and ligands of proteins and nucleic acids, Chem Soc Rev, 40(8) (2011), p. 4346-63.
[75] S.P. Gough, B.O. Petersen, J.O. Duus, Anaerobic chlorophyll isocyclic ring formation in Rhodobacter capsulatus requires a cobalamin cofactor, Proc Natl Acad Sci U S A, 97(12) (2000), p. 6908-13.
[76] J.C. Gonzalez, R.V. Banerjee, S. Huang, J.S. Sumner, R.G. Matthews, Comparison of cobalamin-independent and cobalamin-dependent methionine synthases from Escherichia coli: two solutions to the same chemical problem, Biochemistry, 31(26) (1992), p. 6045-56.
[77] H.M. McGoldrick, C.A. Roessner, E. Raux, A.D. Lawrence, K.J. McLean, A.W. Munro, S. Santabarbara, S.E. Rigby, P. Heathcote, A.I. Scott, M.J. Warren, Identification and characterization of a novel vitamin B12 (cobalamin) biosynthetic enzyme (CobZ) from Rhodobacter capsulatus, containing flavin, heme, and Fe-S cofactors, J Biol Chem, 280(2) (2005), p. 1086-94.
[78] M. Mandal, R.R. Breaker, Gene regulation by riboswitches, Nat Rev Mol Cell Biol, 5(6) (2004), p. 451-63.
[79] J.E. Johnson, Jr., F.E. Reyes, J.T. Polaski, R.T. Batey, B12 cofactors directly stabilize an mRNA regulatory switch, Nature, 492(7427) (2012), p. 133-7.
[80] Z. Cheng, K. Li, L.A. Hammad, J.A. Karty, C.E. Bauer, Vitamin B12 regulates photosystem gene expression via the CrtJ antirepressor AerR in Rhodobacter capsulatus, Mol Microbiol, 91(4) (2014), p. 649-64.
[81] S. Leimkuhler, Shared function and moonlighting proteins in molybdenum cofactor biosynthesis, Biol Chem, 398(9) (2017), p. 1009-1026.
[82] A. Zupok, M. Gorka, B. Siemiatkowska, A. Skirycz, S. Leimkuhler, Iron-Dependent Regulation of Molybdenum Cofactor Biosynthesis Genes in Escherichia coli, J Bacteriol, 201(17) (2019).
[83] A. Zupok, C. Iobbi-Nivol, V. Mejean, S. Leimkuhler, The regulation of Moco biosynthesis and molybdoenzyme gene expression by molybdenum and iron in bacteria, Metallomics, 11(10) (2019), p. 1602-1624.
[84] Y. Stockdreher, S.S. Venceslau, M. Josten, H.G. Sahl, I.A. Pereira, C. Dahl, Cytoplasmic sulfurtransferases in the purple sulfur bacterium Allochromatium vinosum: evidence for sulfur transfer from DsrEFH to DsrC, PLoS One, 7(7) (2012), p. e40785.
[85] O. Genest, V. Mejean, C. Iobbi-Nivol, Multiple roles of TorD-like chaperones in the biogenesis of molybdoenzymes, Fems Microbiol Lett, 297(1) (2009), p. 1-9.
[86] C. Iobbi-Nivol, S. Leimkuhler, Molybdenum enzymes, their maturation and molybdenum cofactor biosynthesis in Escherichia coli, Biochim Biophys Acta, 1827(8-9) (2013), p. 1086-101.
[87] E.E. Regulski, R.H. Moy, Z. Weinberg, J.E. Barrick, Z. Yao, W.L. Ruzzo, R.R. Breaker, A widespread riboswitch candidate that controls bacterial genes involved in molybdenum cofactor and tungsten cofactor metabolism, Mol Microbiol, 68(4) (2008), p. 918-32.
[88] J.K. Rosentel, F. Healy, J.A. Maupin-Furlow, J.H. Lee, K.T. Shanmugam, Molybdate and regulation of mod (molybdate transport), fdhF, and hyc (formate hydrogenlyase) operons in Escherichia coli, J Bacteriol, 177(17) (1995), p. 4857-64.
[89] J. Perard, S. Ollagnier de Choudens, Iron-sulfur clusters biogenesis by the SUF machinery: close to the molecular mechanism understanding, J Biol Inorg Chem, 23(4) (2018), p. 581-596.
[90] P.S. Garcia, S. Gribaldo, B. Py, F. Barras, The SUF system: an ABC ATPase-dependent protein complex with a role in Fe-S cluster biogenesis, Res Microbiol, 170(8) (2019), p. 426-434.
[91] S. Angelini, C. Gerez, S. Ollagnier-de Choudens, Y. Sanakis, M. Fontecave, F. Barras, B. Py, NfuA, a new factor required for maturing Fe/S proteins in Escherichia coli under oxidative stress and iron starvation conditions, J Biol Chem, 283(20) (2008), p. 14084-91.

[92] M. Diender, R. Pereira, H.J. Wessels, A.J. Stams, D.Z. Sousa, Proteomic Analysis of the Hydrogen and Carbon Monoxide Metabolism of Methanothermobacter marburgensis, Front Microbiol, 7 (2016), p. 1049.
[93] L. Rajeev, K.L. Hillesland, G.M. Zane, A. Zhou, M.P. Joachimiak, Z. He, J. Zhou, A.P. Arkin, J.D. Wall, D.A. Stahl, Deletion of the Desulfovibrio vulgaris carbon monoxide sensor invokes global changes in transcription, J Bacteriol, 194(21) (2012), p. 5783-93.
[94] S.N. Parshina, J. Sipma, A.M. Henstra, A.J. Stams, Carbon monoxide as an electron donor for the biological reduction of sulphate, Int J Microbiol, 2010 (2010), p. 319527.
[95] Y.J. Moon, J. Kwon, S.H. Yun, H.L. Lim, M.S. Kim, S.G. Kang, J.H. Lee, J.S. Choi, S.I. Kim, Y.H. Chung, Proteome analyses of hydrogen-producing hyperthermophilic archaeon Thermococcus onnurineus NA1 in different one-carbon substrate culture conditions, Mol Cell Proteomics, 11(6) (2012), p. M111 015420.
[96] Y. Fukuyama, K. Omae, T. Yoshida, Y. Sako, Transcriptome analysis of a thermophilic and hydrogenogenic carboxydotroph Carboxydothermus pertinax, Extremophiles, 23(4) (2019), p. 389-398.
[97] L.K. Wareham, R. Begg, H.E. Jesse, J.W.A. van Beilen, S. Ali, D. Svistunenko, S. McLean, K.J. Hellingwerf, G. Sanguinetti, R.K. Poole, Carbon Monoxide Gas Is Not Inert, but Global, in Its Consequences for Bacterial Gene Expression, Iron Acquisition, and Antibiotic Resistance, Antioxid Redox Sign, 24(17) (2016), p. 1013-1028.
[98] S. McLean, R. Begg, H.E. Jesse, B.E. Mann, G. Sanguinetti, R.K. Poole, Analysis of the bacterial response to Ru(CO)3Cl(Glycinate) (CORM-3) and the inactivated compound identifies the role played by the ruthenium compound and reveals sulfur-containing species as a major target of CORM-3 action, Antioxid Redox Signal, 19(17) (2013), p. 1999-2012.
[99] K.S. Davidge, G. Sanguinetti, C.H. Yee, A.G. Cox, C.W. McLeod, C.E. Monk, B.E. Mann, R. Motterlini, R.K. Poole, Carbon monoxide-releasing antibacterial molecules target respiration and global transcriptional regulators, J Biol Chem, 284(7) (2009), p. 4516-24.
[100] J.D. Fox, R.L. Kerby, G.P. Roberts, P.W. Ludden, Characterization of the CO-induced, CO-tolerant hydrogenase from Rhodospirillum rubrum and the gene encoding the large subunit of the enzyme, J Bacteriol, 178(6) (1996), p. 1515-24.
[101] R.L. Kerby, G.P. Roberts, Sustaining N2-dependent growth in the presence of CO, J Bacteriol, 193(3) (2011), p. 774-7.
[102] J. Butcher, S. Sarvan, J.S. Brunzelle, J.F. Couture, A. Stintzi, Structure and regulon of Campylobacter jejuni ferric uptake regulator Fur define apo-Fur regulation, Proc Natl Acad Sci U S A, 109(25) (2012), p. 10047-52.
[103] L. Pecqueur, B. D'Autreaux, J. Dupuy, Y. Nicolet, L. Jacquamet, B. Brutscher, I. Michaud-Soret, B. Bersch, Structural changes of Escherichia coli ferric uptake regulator during metal-dependent dimerization and activation explored by NMR and X-ray crystallography, J Biol Chem, 281(30) (2006), p. 21286-95.
[104] J. Katigbak, Y. Zhang, Iron Binding Site in a Global Regulator in Bacteria - Ferric Uptake Regulator (Fur) Protein: Structure, Mossbauer Properties, and Functional Implication, J Phys Chem Lett, 2012(3) (2012), p. 3503-3508.
[105] Y.J. An, B.E. Ahn, A.R. Han, H.M. Kim, K.M. Chung, J.H. Shin, Y.B. Cho, J.H. Roe, S.S. Cha, Structural basis for the specialization of Nur, a nickel-specific Fur homolog, in metal sensing and DNA recognition, Nucleic Acids Res, 37(10) (2009), p. 3442-51.
[106] D.A. Traore, A. El Ghazouani, S. Ilango, J. Dupuy, L. Jacquamet, J.L. Ferrer, C. Caux-Thang, V. Duarte, J.M. Latour, Crystal structure of the apo-PerR-Zn protein from Bacillus subtilis, Mol Microbiol, 61(5) (2006), p. 1211-9.
[107] N. Makthal, S. Rastegari, M. Sanson, Z. Ma, R.J. Olsen, J.D. Helmann, J.M. Musser, M. Kumaraswami, Crystal structure of peroxide stress regulator from Streptococcus pyogenes provides functional insights into the mechanism of oxidative stress sensing, J Biol Chem, 288(25) (2013), p. 18311-24.
[108] Y. Perez-Riverol, A. Csordas, J. Bai, M. Bernal-Llinares, S. Hewapathirana, D.J. Kundu, A. Inuganti, J. Griss, G. Mayer, M. Eisenacher, E. Pérez, J. Uszkoreit, J. Pfeuffer, T. Sachsenberg, S. Yilmaz, S. Tiwary, J. Cox, E. Audain, M. Walzer, A.F. Jarnuczak, T. Ternent, A. Brazma, J.A. Vizcaíno, The PRIDE database and related tools and resources in 2019: improving support for quantification data, Nucleic Acids Res, 47(D1) (2019), p. D442-d450.

Supplementary material:

Συππλεμ ενταρψ Ταβλε 2: Λιστ οφ προτεινσ σιγ νιφψκαντλψ μ οδυλατεδ βψ ΧΟ εξποσυρε (Υ□2), ασ δε τερμ ινεδ βψ τηε σηοτγυν προτεομ ιχ αναλψσισ

accession	gene_name	description	ρατιο ΧΟ/χτρλ	U (Mann Whitney U test)	t-test_g1_vs_g2	χοσε ρεγ ε	#πεπτιδεσ
Q2RNM9	Rru_A3472	Nucleoid-associated protein Rru_A3472 GN=Rru_A3472 PE=3 SV=1	9,65E-07	0	2,11E-02	24,3	2
Q2RRY5	Rru_A2310	Cytochrome c family protein GN=Rru_A2310 PE=4 SV=1	1,25E-06	0	3,08E-03	10,42	2
Q2RU12	Rru_A1583	Chemotaxis sensory transducer GN=Rru_A1583 PE=4 SV=1	1,80E-06	0	2,47E-02	8,4	4
Q2RVQ1	Rru_A0993	Transcriptional regulator, NifA, Fis family GN=Rru_A0993 PE=4 SV=1	1,94E-06	0	7,32E-05	3,17	2
Q2RUW8	Rru_A1276	ATP-cone GN=Rru_A1276 PE=4 SV=1	2,21E-06	0	4,43E-03	5,79	2
Q2RX46	Rru_A0494	Phytoene synthase GN=Rru_A0494 PE=4 SV=1	2,87E-06	0	3,09E-04	5,56	2
Q2RXL8	Rru_A0322	Peptidase M52, hydrogen uptake protein GN=Rru_A0322 PE=4 SV=1	2,88E-06	0	7,35E-04	12,34	2
Q2RQH0	Rru_A2828	Uncharacterized protein GN=Rru_A2828 PE=4 SV=1	3,13E-06	0	2,15E-01	11,83	2
Q2RTB0	Rru_A1835	Butyryl-CoA dehydrogenase GN=Rru_A1835 PE=3 SV=1	3,24E-06	0	1,45E-05	8,44	2
Q2RQS3	Rru_A2725	Multi-sensor hybrid histidine kinase GN=Rru_A2725 PE=4 SV=1	3,35E-06	0	6,41E-04	2,4	2
Q2RXI2	Rru_A0358	Heme oxygenase GN=Rru_A0358 PE=4 SV=1	3,37E-06	1,5	2,21E-02	10,5	2
Q2RXP1	Rru_A0299	Glutamine amidotransferase class-I GN=Rru_A0299 PE=4 SV=1	3,53E-06	0	3,35E-03	15,83	2
Q2RQ53	Rru_A2945	Uncharacterized protein GN=Rru_A2945 PE=4 SV=1	4,05E-06	0	7,07E-03	18,29	2
Q2RNV7	Rru_A3394	Uncharacterized protein GN=Rru_A3394 PE=4 SV=1	4,17E-06	0	2,02E-02	21,1	3
Q2RR06	Rru_A2642	Alpha/beta hydrolase fold GN=Rru_A2642 PE=4 SV=1	5,91E-06	0	6,49E-03	7,87	2
Q2RN56	Rru_A3645	NAD-dependent protein deacylase GN=cobB PE=3 SV=1	1,33E-05	1,5	2,62E-02	12,35	2
Q2RPF6	Rru_A3194	SMF protein GN=Rru_A3194 PE=4 SV=1	4,12E-02	0	3,13E-04	26,74	8
Q2RSN4	Rru_A2061	Uncharacterized protein GN=Rru_A2061 PE=4 SV=1	5,31E-02	0	9,30E-03	19,61	3
Q2RPX6	Rru_A3024	Prolyl 4-hydroxylase, alpha subunit GN=Rru_A3024 PE=4 SV=1	7,56E-02	0	4,67E-04	25,48	5
Q2RTC8	Rru_A1817	TPR repeat GN=Rru_A1817 PE=4 SV=1	9,57E-02	0	1,49E-02	10,26	9
Q2RS37	Rru_A2258	Uncharacterized protein GN=Rru_A2258 PE=4 SV=1	9,66E-02	0	2,40E-03	15,64	4
Q2RV51	Rru_A1193	Dinitrogenase iron-molybdenum cofactor biosynthesis GN=Rru_A1193 PE=4 SV=1	1,14E-01	0	9,68E-04	37,14	3
Q2RRF3	Rru_A2492	Glycosyl transferase, group 1 GN=Rru_A2492 PE=4 SV=1	1,22E-01	0	4,75E-04	13,75	2
Q2RVJ3	Rru_A1051	N5-carboxyaminoimidazole ribonucleotide synthase GN=purK PE=3 SV=1	1,22E-01	0	5,90E-03	16,48	3
Q2RX19	Rru_A0522	Response regulator receiver domain protein (CheY) GN=Rru_A0522 PE=4 SV=1	1,27E-01	0	1,64E-03	26,02	2
Q2RRY6	Rru_A2309	NADH peroxidase GN=Rru_A2309 PE=4 SV=1	1,43E-01	0	2,28E-03	73,1	31
Q2RXD1	Rru_A0409	Alanine racemase GN=alr PE=3 SV=1	1,44E-01	2	7,45E-02	30,75	7
Q2RV52	Rru_A1192	Ubiquinol-cytochrome c reductase iron-sulfur subunit GN=Rru_A1192 PE=4 SV=1	1,52E-01	0	8,09E-08	31,91	5
Q2RNC5	Rru_A3576	UDP-glucuronate 5'-epimerase GN=Rru_A3576 PE=4 SV=1	1,98E-01	0	2,21E-03	17,91	4
Q2RRF6	Rru_A2489	Catalase GN=Rru_A2489 PE=4 SV=1	2,12E-01	0	6,60E-04	15,29	4
Q2RVV4	Rru_A0940	DNA repair protein RecN GN=Rru_A0940 PE=3 SV=1	2,67E-01	0	1,44E-02	16,46	6
Q2RPM5	Rru_A3125	Glycosyl transferase, group 1 GN=Rru_A3125 PE=4 SV=1	2,74E-01	0	1,32E-03	8,37	3
Q2RVW0	Rru_A0934	Uncharacterized protein GN=Rru_A0934 PE=4 SV=1	2,74E-01	0	1,37E-06	22,69	8
Q2RV68	Rru_A1176	Histone deacetylase superfamily GN=Rru_A1176 PE=4 SV=1	2,83E-01	0	1,26E-05	49,12	7
Q2RQ54	Rru_A2944	ArgK protein GN=Rru_A2944 PE=4 SV=1	2,83E-01	0	1,11E-04	6,27	2
Q2RWG8	Rru_A0723	Amine oxidase GN=Rru_A0723 PE=4 SV=1	3,20E-01	0	5,54E-04	8,24	2
Q2RSH6	Rru_A2119	Molybdopterin oxidoreductase GN=Rru_A2119 PE=3 SV=1	3,32E-01	2	4,87E-02	10,89	6
Q2RQQ1	Rru_A2747	Short-chain dehydrogenase/reductase SDR GN=Rru_A2747 PE=4 SV=1	3,38E-01	0	4,63E-05	14,62	3
Q2RQE7	Rru_A2851	Uncharacterized protein GN=Rru_A2851 PE=4 SV=1	3,42E-01	0	4,34E-02	26,12	3
Q2RTV0	Rru_A1645	Uncharacterized protein GN=Rru_A1645 PE=4 SV=1	3,42E-01	0	4,28E-06	10,48	2
Q8GDE1	Rru_A2996	Cobalt-precorrin-5B C(1)-methyltransferase GN=cbiD PE=3 SV=1	3,45E-01	0	3,31E-04	13,45	2
Q2RY66	Rru_A0124	Putative diguanylate phosphodiesterase (EAL domain) GN=Rru_A0124 PE=4 SV=1	3,51E-01	0	6,65E-04	7,35	4
Q2RWD4	Rru_A0757	Isochorismatase hydrolase GN=Rru_A0757 PE=4 SV=1	3,55E-01	0	1,08E-05	33,51	3
Q2RT62	Rru_A1883	Magnesium transport protein CorA GN=corA PE=3 SV=1	3,56E-01	1	1,95E-02	6,04	2
Q2RPT9	Rru_A3061	Uncharacterized protein GN=Rru_A3061 PE=4 SV=1	3,66E-01	0	1,42E-04	7,84	2
Q2RNU6	Rru_A3405	S-(hydroxymethyl)glutathione dehydrogenase GN=Rru_A3405 PE=3 SV=1	3,85E-01	0	2,87E-04	16,13	5
Q2RVS8	Rru_A0966	Xanthine dehydrogenase, molybdenum binding subunit apoprotein GN=Rru_A0966 PE=4 SV=1	3,86E-01	0	5,42E-03	6,1	4
Q2RT68	Rru_A1877	Lipoyl synthase GN=lipA PE=3 SV=1	3,91E-01	0	8,32E-03	9,55	2
Q2RWW1	Rru_A0580	OsmC-like protein GN=Rru_A0580 PE=4 SV=1	4,10E-01	0	4,92E-04	47,22	4
Q2RY92	Rru_A0098	Cystathionine gamma-synthase GN=Rru_A0098 PE=3 SV=1	4,29E-01	0	9,78E-04	18,36	5
Q2RWQ9	Rru_A0632	Chemotaxis sensory transducer GN=Rru_A0632 PE=4 SV=1	4,31E-01	0	2,71E-03	3,94	2
Q2RY31	Rru_A0159	Exodeoxyribonuclease 7 large subunit GN=xseA PE=3 SV=1	4,32E-01	0	5,93E-05	8,38	3
Q2RU23	Rru_A1572	Methylmalonyl-CoA epimerase GN=Rru_A1572 PE=4 SV=1	4,34E-01	0	5,12E-02	47,76	4
Q2RPJ5	Rru_A3155	Uncharacterized protein GN=Rru_A3155 PE=4 SV=1	4,38E-01	1	1,52E-02	9,55	2
Q2RVH3	Rru_A1071	Adenylate/guanylate cyclase GN=Rru_A1071 PE=4 SV=1	4,47E-01	0	1,05E-03	19,26	9
Q2RVI7	Rru_A1057	3-hydroxybutyrate dehydrogenase GN=Rru_A1057 PE=4 SV=1	4,50E-01	0	3,10E-03	19,31	4
Q2RQR9	Rru_A2729	Uncharacterized protein GN=Rru_A2729 PE=4 SV=1	4,52E-01	0	1,03E-02	38,5	6
Q2RSR0	Rru_A2035	Phosphate binding protein, putative GN=Rru_A2035 PE=4 SV=1	4,54E-01	1	9,07E-03	9,47	2
Q2RRN2	Rru_A2413	Poly(R)-hydroxyalkanoic acid synthase, class I GN=Rru_A2413 PE=4 SV=1	4,57E-01	0	4,09E-05	48,66	22
Q2RU16	Rru_A1579	Lipoprotein-releasing system ATP-binding protein LolD 1 GN=lolD1 PE=3 SV=2	4,60E-01	2	7,12E-02	25,22	3
Q9RDT6	Rru_A1816	PHA synthase GN=phaCRr PE=4 SV=1	4,63E-01	0	6,34E-05	30,41	15
Q2RRZ2	Rru_A2303	Deoxyribose-phosphate aldolase GN=deoC PE=3 SV=1	4,68E-01	0	2,30E-03	36,97	6
Q2RQN8	Rru_A2760	Uncharacterized protein GN=Rru_A2760 PE=4 SV=1	4,69E-01	0	1,22E-03	26,67	2
Q2RSL3	Rru_A2082	Hemerythrin HHE cation binding region GN=Rru_A2082 PE=4 SV=1	4,75E-01	0	5,12E-03	26,79	4
Q2RWE1	Rru_A0750	Peptide chain release factor 1 GN=prfA PE=3 SV=1	4,82E-01	0	1,64E-04	19,77	5
Q2RRH2	Rru_A2473	PAS/PAC sensor signal transduction histidine kinase GN=Rru_A2473 PE=4 SV=1	4,82E-01	0	1,99E-03	5,09	3
Q2RTC0	Rru_A1825	Riboflavin biosynthesis protein RibD GN=Rru_A1825 PE=3 SV=1	4,85E-01	0	4,01E-06	9,26	3
Q2RN96	Rru_A3605	Iron-sulfur cluster binding protein GN=Rru_A3605 PE=4 SV=1	4,85E-01	0	1,45E-04	4,45	2
Q2RXK6	Rru_A0334	Transcriptional regulator, LysR family GN=Rru_A0334 PE=3 SV=1	4,89E-01	0	3,42E-04	8,12	2
Q2RYC9	Rru_A0061	Purine and other phosphorylases, family 1 GN=Rru_A0061 PE=4 SV=1	4,93E-01	0	4,06E-03	32,23	6
Q2RQN4	Rru_A2764	Uncharacterized protein GN=Rru_A2764 PE=4 SV=1	4,94E-01	0	3,14E-04	8,18	3
Q2RRI1	Rru_A2464	Hydroxypyruvate reductase GN=Rru_A2464 PE=4 SV=1	4,94E-01	0	9,96E-04	6,18	2
Q2RQJ7	Rru_A2811	Ribosomal protein S12 methylthiotransferase RimO GN=rimO PE=3 SV=1	4,97E-01	0	5,89E-04	16,1	5
Q2RQ87	Rru_A2911	ABC-type uncharacterized transport system auxiliary component-like GN=Rru_A2911 PE=4 SV=1	4,97E-01	0	1,85E-04	39,9	5
Q2RN79	Rru_A3622	Uncharacterized protein GN=Rru_A3622 PE=4 SV=1	5,05E-01	0	1,70E-04	4,41	3
Q2RXD7	Rru_A0403	Short-chain dehydrogenase/reductase SDR GN=Rru_A0403 PE=4 SV=1	5,08E-01	0	2,76E-03	75,53	13
Q2RNR0	Rru_A3441	Transcriptional regulator, PadR family GN=Rru_A3441 PE=4 SV=1	5,09E-01	1	6,54E-03	58,33	8
Q2RPN5	Rru_A3115	ATPase GN=Rru_A3115 PE=4 SV=1	5,17E-01	0	1,17E-03	7,33	2
Q2RY89	Rru_A0101	Uncharacterized protein GN=Rru_A0101 PE=4 SV=1	5,17E-01	0	4,69E-03	16,84	2
Q2RU15	Rru_A1580	GCN5-related N-acetyltransferase GN=Rru_A1580 PE=4 SV=1	5,18E-01	1	1,21E-02	17,93	2
Q2RQT9	Rru_A2709	Thioesterase superfamily GN=Rru_A2709 PE=4 SV=1	5,21E-01	0	6,77E-04	18,67	2
Q2RMQ8	Rru_A3793	Molybdopterin biosynthesis protein GN=Rru_A3793 PE=4 SV=1	5,22E-01	0	3,58E-03	25,83	5
Q2RXK1	Rru_A0339	Short-chain dehydrogenase/reductase SDR GN=Rru_A0339 PE=4 SV=1	5,25E-01	0	4,71E-05	11,03	2
Q2RQF5	Rru_A2843	Flagellar basal-body rod protein FlgG GN=Rru_A2843 PE=3 SV=1	5,26E-01	0	1,12E-04	42,53	6
Q2RXJ4	Rru_A0346	CRISPR-associated protein, CT1974 family GN=Rru_A0346 PE=4 SV=1	5,28E-01	0	3,45E-03	25,1	5
Q2RSA2	Rru_A2193	Abc1 protein GN=Rru_A2193 PE=4 SV=1	5,29E-01	0	4,67E-05	20,58	7
Q2RSR6	Rru_A2029	Serine O-acetyltransferase GN=Rru_A2029 PE=4 SV=1	5,37E-01	0	1,51E-03	26,38	5
Q2RVF1	Rru_A1093	Uncharacterized protein GN=Rru_A1093 PE=4 SV=1	5,42E-01	0	1,93E-04	6,45	2
Q2RTQ8	Rru_A1687	Inositol monophosphatase GN=Rru_A1687 PE=4 SV=1	5,45E-01	0	3,08E-03	29,41	6
Q2RRM5	Rru_A2420	Transferase hexapeptide repeat GN=Rru_A2420 PE=4 SV=1	5,46E-01	0	7,15E-04	52,91	5
Q2RPH7	Rru_A3173	Transcriptional regulator, TetR family GN=Rru_A3173 PE=4 SV=1	5,52E-01	0	9,50E-03	15,49	2
Q2RWC2	Rru_A0769	Extracellular solute-binding protein, family 1 GN=Rru_A0769 PE=4 SV=1	5,52E-01	2	1,40E-02	19,31	4
Q2RT29	Rru_A1916	Ferredoxin GN=Rru_A1916 PE=4 SV=1	5,55E-01	2	1,30E-01	18,11	2
Q2RY29	Rru_A0161	10 kDa chaperonin GN=groS PE=3 SV=1	5,60E-01	1	1,76E-02	71,15	6
Q2RNY4	Rru_A3367	Cob(I)yrinic acid a,c-diamide adenosyltransferase GN=Rru_A3367 PE=3 SV=1	5,60E-01	0	1,31E-05	25,58	4
Q2RNY9	Rru_A3362	Uroporphyrinogen-III C-methyltransferase GN=Rru_A3362 PE=3 SV=1	5,62E-01	0	1,34E-03	20,96	5

Supplementary Table 2: List of proteins significantly modulated by CO exposure (U≤2), as determined by the shotgun proteomic analysis

Supplementary Table 4: Quantitative and identification data for proteins identified as modulated through the 2D gel-based proteomic analysis.
For proteins represented by multiple spots, they are numbered from the most basic to the most acidic

protein identifier	ratio CO/ctrl	p value	Protein name	Protein accession numbers	Protein molecular weight (Da)	Exclusive unique peptide count	Percentage sequence coverage
acat	0,759	0,0028	Acetyl-CoA acetyltransferase	Q2RXR6| Q2RXR6_RHORT	40 190,6	18	63%
accC	0,674	0,0004	Biotin carboxylase	Q2RYD8| Q2RYD8_RHORT	72 789,9	16	27%
Ahcy	0,861	0,0015	Adenosylhomocysteinase	Q2RNQ7| Q2RNQ7_RHORT	50 617,3	5	12%
AhpC	1,234	0,0004	Alkyl hydroperoxide reductase/ Thiol specific antioxidant	Q2RUH6| Q2RUH6_RHORT	20 587,8	15	74%
aldo/1	1,369	0,0011	Fructose-1,6-bisphosphate aldolase	Q2RWU5| Q2RWU5_RHORT	38 154,7	4	11%
aldo/2	0,853	0,0028	Fructose-1,6-bisphosphate aldolase	Q2RWU5| Q2RWU5_RHORT	38 154,7	14	36%
aldo/3	0,616	0,0004	Fructose-1,6-bisphosphate aldolase	Q2RWU5| Q2RWU5_RHORT	38 154,7	10	30%
APRT	1,484	0,0036	Adenine phosphoribosyltransferase	Q2RWT4| APT_RHORT	18 312,9	7	45%
ATPB	1,185	0,0084	ATP synthase subunit beta	P05038| ATPB_RHORU,Q2RV18| ATPB_RHORT	50 852,7	20	62%
ATPE	1,251	0,0237	ATP synthase epsilon chain	P05442| ATPE_RHORU,Q2RV17| ATPE_RHORT	14 307,1	5	52%
BamA	0,75	0,0042	Outer membrane protein assembly factor BamA	Q2RU01| Q2RU01_RHORT	87 285,2	28	39%
bchx	0,878	0,0043	Chlorophyllide reductase iron protein subunit X	Q2RQ20| Q2RQ20_RHORT	33 799,2	14	46%
BFR	1,426	0,0021	Bacterioferritin	Q2RSA0| Q2RSA0_RHORT	18 042,3	4	33%
CBL	0,831	0,0005	Cystathionine beta-lyase	Q2RTY2| Q2RTY2_RHORT	42 687,2	11	35%
cbs/1	1,139	0,0235	CBS domain protein	Q2RMS8| Q2RMS8_RHORT	34 963,0	7	22%
cbs/2	0,788	0,0029	CBS domain protein	Q2RMS8| Q2RMS8_RHORT	34 963,0	7	21%
CH105	0,778	0,0189	10 kDa chaperonin	Q2RWV5| Q2RWV5_RHORT	10 211,1	7	64%
ch601	1,263	0,0194	60 kDa chaperonin 1	Q2RY28| CH601_RHORT	57 044,7	23	56%
ch602	1,254	0,0098	60 kDa chaperonin 2	Q2RWV4| CH602_RHORT	57 636,4	15	50%
cold shock1	0,612	0,0007	Cold-shock DNA-binding protein family	Q2RNN9| Q2RNN9_RHORT	21 559,9	12	58%
cold shock2	0,561	0,0171	Cold-shock DNA-binding protein family	Q2RU74| Q2RU74_RHORT	7316,3	3	68%
CooC/1	3,734	<0,0001	Carbon monoxide dehydrogenase accessory protein CooC	P31897| COOC_RHORU,Q2RUG6| Q2RUG6_RHORT	27 762,9	9	39%
CooC/2	2,929	<0,0001	Carbon monoxide dehydrogenase accessory protein CooC	P31897| COOC_RHORU,Q2RUG6| Q2RUG6_RHORT	27 762,9	9	39%
CooC/3	1,736	0,0048	Carbon monoxide dehydrogenase accessory protein CooC	P31897| COOC_RHORU,Q2RUG6| Q2RUG6_RHORT	27 762,9	6	24%
CooS/1	27	<0,0001	Carbon monoxide dehydrogenase	P31896| COOS_RHORU,Q2RUG7| Q2RUG7_RHORT	66 854,4	17	32%
CooS/2	26	<0,0001	Carbon monoxide dehydrogenase	P31896| COOS_RHORU,Q2RUG7| Q2RUG7_RHORT	66 854,4	18	37%
CooS/3	116	<0,0001	Carbon monoxide dehydrogenase	P31896| COOS_RHORU,Q2RUG7| Q2RUG7_RHORT	66854,4	18	35%
CooT	21,312	0,0025	CooT	P72320| P72320_RHORU,Q2RUG5| Q2RUG5_RHORT	7 096,0	3	61%
crtF	0,677	<0,0001	Hydroxyneurosporene-O-methyltransferase	Q2RQ18| Q2RQ18_RHORT,Q8GDC7| Q8GDC7_RHORU	42 447,7	14	33%
DHOM	0,656	0,0047	Homoserine dehydrogenase	Q2RRN5| Q2RRN5_RHORT	45 046,3	13	36%
DPS	1,324	0,004	Ferritin and Dps	Q2RXK7| Q2RXK7_RHORT	17 661,8	8	60%
DSTOR	0,575	0,0189	Trimethylamine-N-oxide reductase (Cytochrome c)	Q2RUV7| Q2RUV7_RHORT	89 341,5	33	50%
efp	1,37	0,0022	Elongation factor P	Q2RVG7| EFP_RHORT	20 798,4	7	42%
ETF	1,136	0,0022	Electron transfer flavoprotein	Q2RPS2| Q2RPS2_RHORT	31 447,7	8	39%
ETFB/1	1,342	0,0026	Electron transfer flavoprotein beta-subunit	Q2RPS3| Q2RPS3_RHORT	26 644,4	7	33%
ETFB/2	2,138	<0,0001	Electron transfer flavoprotein beta-subunit	Q2RPS3| Q2RPS3_RHORT	26 644,4	9	41%
fabG/1	0,824	0,002	3-oxoacyl-[acyl-carrier-protein] reductase	Q2RXR7| Q2RXR7_RHORT	25 834,7	11	60%
fabG/2	0,73	0,0023	3-oxoacyl-[acyl-carrier-protein] reductase	Q2RXR7| Q2RXR7_RHORT	25 834,7	8	44%
Flagellin	1,188	0,0019	Flagellin	Q2RRB1| Q2RRB1_RHORT	30 682,8	10	41%
FliK	0,668	0,0017	Flagellar hook-length control protein	Q2RWZ3| Q2RWZ3_RHORT	60 791,8	17	49%
FMN-Red	0,621	0,001	NADPH-dependent FMN reductase	Q2RPR7| Q2RPR7_RHORT	20 022,2	8	55%
GAPDH/1	0,605	0,0017	Glyceraldehyde-3-phosphate dehydrogenase	Q2RXW8| Q2RXW8_RHORT	35 583,5	8	26%
GAPDH/2	0,789	0,003	Glyceraldehyde-3-phosphate dehydrogenase	Q2RXW8| Q2RXW8_RHORT	35 583,5	16	61%
GAPDH/3	0,86	0,0008	Glyceraldehyde-3-phosphate dehydrogenase	Q2RXW8| Q2RXW8_RHORT	35 583,5	18	66%
GlnJ	0,435	0,0023	Nitrogen regulatory protein P-II	Q2RVB4| Q2RVB4_RHORT,Q9AM71| Q9AM71_RHORU	12 283,3	4	37%
hemB	0,757	0,0013	Delta-aminolevulinic acid dehydratase	Q2RTA8| Q2RTA8_RHORT	36 476,1	7	23%
hemC	0,858	0,0019	Porphobilinogen deaminase	Q2RND3| Q2RND3_RHORT	34 156,7	13	42%
His8/1	1,157	0,0048	Histidinol-phosphate aminotransferase	Q2RP86| HIS8_RHORT	39 049,8	5	15%
His8/2	1,607	<0,0001	Histidinol-phosphate aminotransferase	Q2RP86| HIS8_RHORT	39 049,8	5	17%
His8/3	1,2	0,0024	Histidinol-phosphate aminotransferase	Q2RP86| HIS8_RHORT	39 049,8	8	27%
ISPG	0,821	0,0473	4-hydroxy-3-methylbut-2-en-1-yl diphosphate synthase (flavodoxin)	Q2RWE4| ISPG_RHORT	40 785,4	11	32%
LacI	0,798	0,0037	Periplasmic binding protein/LacI transcriptional regulator	Q2RUQ8| Q2RUQ8_RHORT	35 656,3	16	51%
Leu1	1,25	0,0338	2-isopropylmalate synthase	Q2RT17| LEU1_RHORT	61 147,4	2	4%
LHA	1,654	0,0021	Light-harvesting protein B-870 alpha chain	P02947| LHA_RHORU,Q2RQ24| Q2RQ24_RHORT	7 107,7	2	29%
MDH	1,155	0,0444	Malate dehydrogenase	Q2RV34| MDH_RHORT	33 479,2	14	58%
modA	1,29	0,0027	Molybdenum ABC transporter, periplasmic binding protein	Q2RWI7| Q2RWI7_RHORT	26 899,6	11	50%
NifU	0,539	0,0014	Nitrogen-fixing NifU-like	Q2RNH0| Q2RNH0_RHORT	19 473,2	7	39%
NPD	0,546	0,0007	2-nitropropane dioxygenase, NPD	Q2RMR4| Q2RMR4_RHORT	51 374,2	13	33%
NPR/1	0,368	0,001	NADH peroxidase	Q2RRY6| Q2RRY6_RHORT	58 619,7	13	29%
NPR/2	0,31	<0,0001	NADH peroxidase	Q2RRY6| Q2RRY6_RHORT	58 619,7	18	36%
NuoC/1	0,847	0,0005	NADH-quinone oxidoreductase subunit C	Q2RU38| NUOC_RHORT	24 847,1	12	66%
NuoC/2	0,585	0,0005	NADH-quinone oxidoreductase subunit C	Q2RU38| NUOC_RHORT	24 847,1	8	43%
NuoD	1,448	0,001	NADH-quinone oxidoreductase subunit D	Q2RU37| NUOD_RHORT	44 279,6	4	11%
PAL	2,07	0,0025	Peptidoglycan-associated protein	Q2RVE9| Q2RVE9_RHORT	17 124,7	3	22%
PepSY	1,197	0,0135	Propeptide, PepSYamd peptidase M4	Q2RQ86| Q2RQ86_RHORT	26870,1	13	60%
PFK	0,783	0,0003	ATP-dependent 6-phosphofructokinase	Q2RVJ7| Q2RVJ7_RHORT	38 860,4	15	52%
phasin/1	1,111	0,055	Phasin	Q2RP67| Q2RP67_RHORT,Q8GD50| Q8GD50_RHORU	17 538,0	11	65%
phasin/2	0,78	0,0026	Phasin	Q2RP67| Q2RP67_RHORT,Q8GD50| Q8GD50_RHORU	17 538,0	9	61%
PNTAA	0,723	<0,0001	NAD(P) transhydrogenase subunit alpha part 1	P0C186| PNTAA_RHORU,Q2RSB2| PNTAA_RHORT	40 276,7	13	37%
PSPA	0,867	0,0002	Phage shock protein A, PspA	Q2RV26| Q2RV26_RHORT	25 278,9	11	50%
q2rmu9	0,246	<0,001	Uncharacterized protein OS=Rhodospirillum rubrum	Q2RMU9| Q2RMU9_RHORT	14 952,4	3	22%
q2rr88	0,856	0,0008	Uncharacterized protein OS=Rhodospirillum rubrum	Q2RR88| Q2RR88_RHORT	35 007,8	12	43%
q2rrt9 (fgt)	1,971	0,0049	Extracellular solute-binding protein, family 5	Q2RRT9| Q2RRT9_RHORT	59 050,9	6	17%
q2rsp8/1	1,134	0,0005	Extracellular solute-binding protein, family 1	Q2RSP8| Q2RSP8_RHORT	37 902,0	6	22%
q2rsp8/2	0,639	0,0011	Extracellular solute-binding protein, family 1	Q2RSP8| Q2RSP8_RHORT	37 902,0	7	26%
q2rsp8/3	0,306	0,0051	Extracellular solute-binding protein, family 1	Q2RSP8| Q2RSP8_RHORT	37 902,0	6	22%

Supplementary Table 4: **Quantitative and identification data for proteins identified as modulated through the 2D gel-based proteomic analysis.** For proteins represented by multiple spots, they are numbered from the most basic to the most acidic

Supplementary Table 5: List of the pathways in which regulated proteins are encountered.
Pathways in which no more than one protein is found either as up or down regulated were omitted.
Note that a protein can be accounted for in several different pathways.

KEGG pathway	Proteome (shotgun and 2D)	Up	Down
rru00010 Glycolysis / Gluconeogenesis	31	1	8
rru00020 Citrate cycle (TCA cycle)	23	2	1
rru00030 Pentose phosphate pathway	19	4	6
rru00051 Fructose and mannose metabolism	13	4	5
rru00061 Fatty acid biosynthesis	14	2	1
rru00071 Fatty acid degradation	12	1	3
rru00072 Synthesis and degradation of ketone bodies	3	0	2
rru00130 Ubiquinone and other terpenoid-quinone biosynthesis	5	1	2
rru00190 Oxidative phosphorylation	26	4	3
rru00220 Arginine biosynthesis	12	2	1
rru00230 Purine metabolism	38	7	8
rru00240 Pyrimidine metabolism	23	3	3
rru00250 Alanine, aspartate and glutamate metabolism	23	4	5
rru00260 Glycine, serine and threonine metabolism	26	1	4
rru00270 Cysteine and methionine metabolism	31	1	12
rru00280 Valine, leucine and isoleucine degradation	23	1	6
rru00290 Valine, leucine and isoleucine biosynthesis	16	2	1
rru00300 Lysine biosynthesis	13	0	2
rru00310 Lysine degradation	11	1	3
rru00330 Arginine and proline metabolism	16	2	3
rru00340 Histidine metabolism	15	4	3
rru00350 Tyrosine metabolism	6	1	3
rru00360 Phenylalanine metabolism	8	2	3
rru00362 Benzoate degradation	9	1	2
rru00380 Tryptophan metabolism	11	1	4
rru00400 Phenylalanine, tyrosine and tryptophan biosynthesis	19	2	3
rru00401 Novobiocin biosynthesis	3	1	2
rru00450 Selenocompound metabolism	10	1	2
rru00520 Amino sugar and nucleotide sugar metabolism	23	7	2
rru00521 Streptomycin biosynthesis	10	0	2
rru00540 Lipopolysaccharide biosynthesis	13	3	0
rru00541 o-Antigen nucleotide sugar biosynthesis	16	3	2
rru00561 Glycerolipid metabolism	10	2	1
rru00562 Inositol phosphate metabolism	6	0	3
rru00620 Pyruvate metabolism	38	3	5
rru00630 Glyoxylate and dicarboxylate metabolism	36	6	9
rru00633 Nitrotoluene degradation	3	2	0
rru00640 Propanoate metabolism	23	3	7
rru00650 Butanoate metabolism	24	1	7
rru00670 One carbon pool by folate	10	2	1
rru00680 Methane metabolism	25	6	7
rru00710 Carbon fixation in photosynthetic organisms	17	3	8
rru00740 Riboflavin metabolism	7	0	5
rru00760 Nicotinate and nicotinamide metabolism	10	1	3
rru00770 Pantothenate and CoA biosynthesis	15	2	2
rru00790 Folate biosynthesis	10	2	2
rru00860 Porphyrin and chlorophyll metabolism	39	2	8
rru00900 Terpenoid backbone biosynthesis	14	0	3
rru00906 Carotenoid biosynthesis	5	0	3
rru00920 Sulfur metabolism	15	1	3
rru00970 Aminoacyl-tRNA biosynthesis	24	1	5
rru01100 Metabolic pathways	502	62	94
rru01110 Biosynthesis of secondary metabolites	261	23	57
rru01120 Microbial metabolism in diverse environments	137	13	30
rru01200 Carbon metabolism	91	10	22
rru01210 2-Oxocarboxylic acid metabolism	23	4	2
rru01212 Fatty acid metabolism	20	3	3
rru01230 Biosynthesis of amino acids	110	12	21
rru01240 Biosynthesis of cofactors	97	9	23
rru01501 beta-Lactam resistance	10	1	3
rru02010 ABC transporters	58	6	13
rru02020 Two-component system	68	8	10
rru02024 Quorum sensing	37	3	10
rru02030 Bacterial chemotaxis	31	1	3
rru02040 Flagellar assembly	24	1	2
rru02060 Phosphotransferase system (PTS)	5	2	0
rru03010 Ribosome	50	7	1
rru03018 RNA degradation	14	7	1
rru03430 Mismatch repair	11	0	3

Supplementary Table 5: **List of the pathways in which regulated proteins are encountered.** Pathways in which no more than one protein is found either as up or down regulated were omitted. Note that a protein can be accounted for in several different pathways.

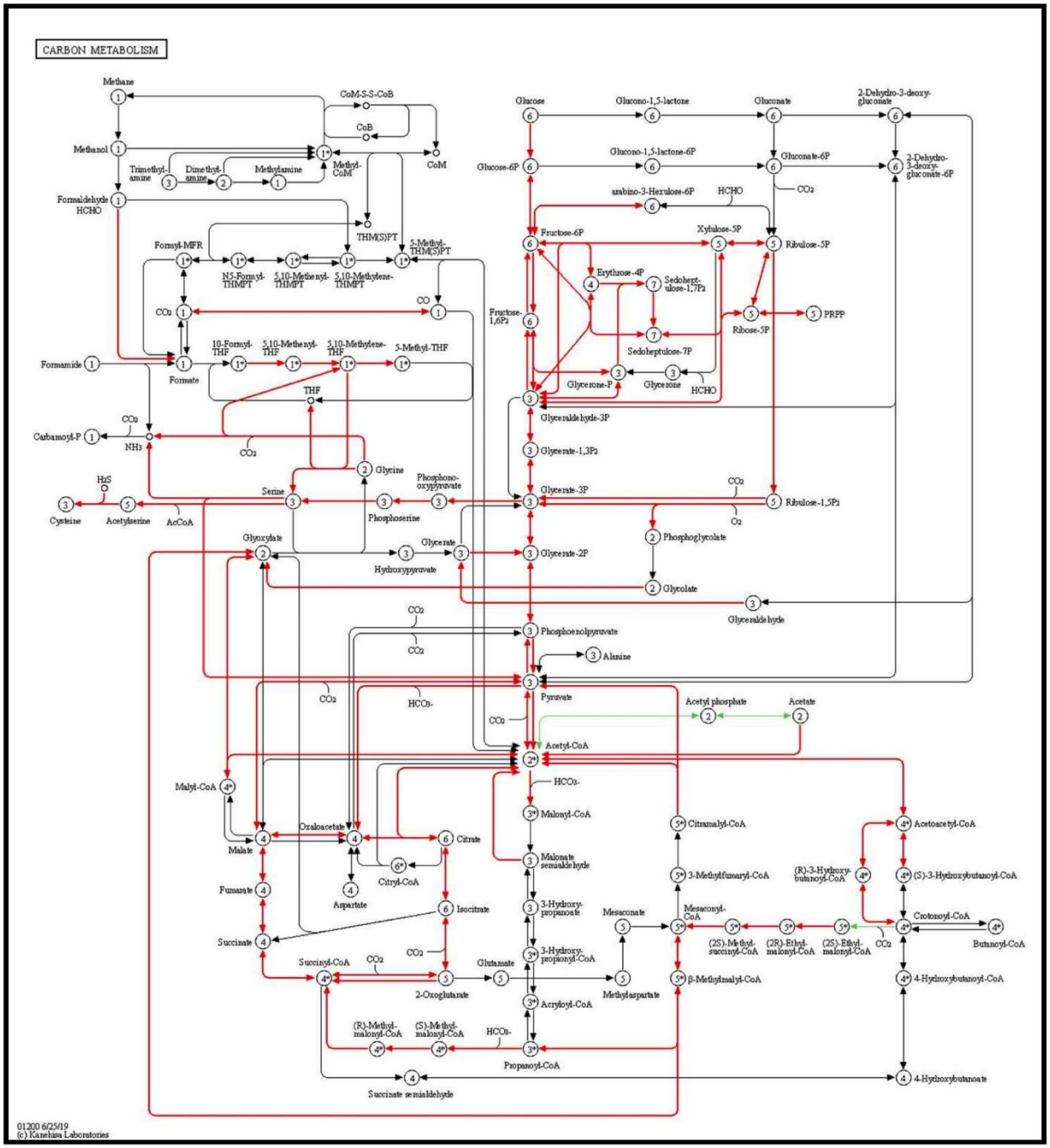

Supplementary Figure 1 : Carbon metabolism (rru01200)
This figure was made with KEGG mapper (https://www.genome.jp/kegg/mapper.html), red arrows representing the proteins found in our study (shotgun and 2D approaches) and green the proteins predicted based on the genome but not experimentally detected.

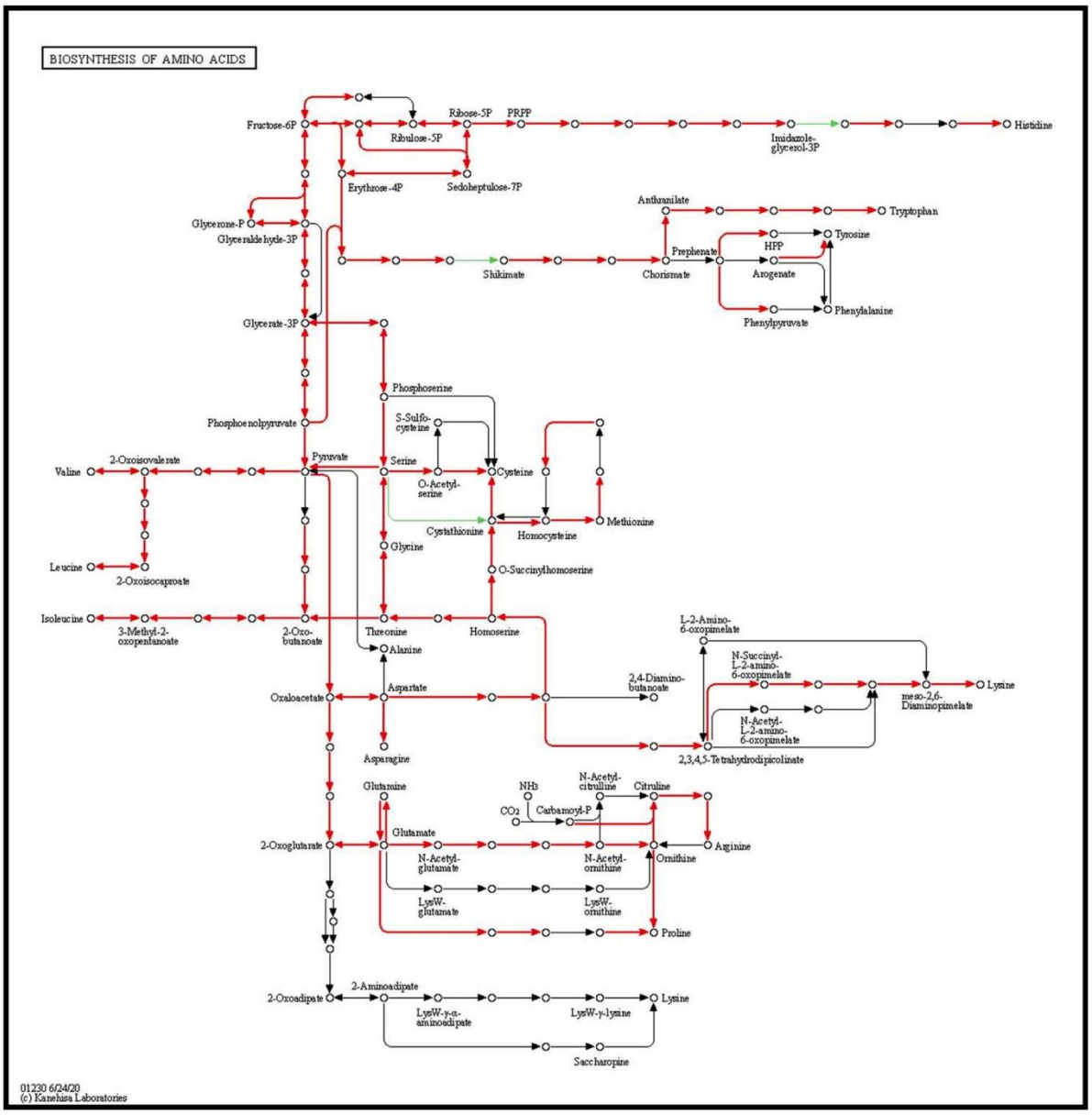

Supplementary Figure 2 : Biosynthesis of amino acids (rru01230)
This figure was made with KEGG mapper (https://www.genome.jp/kegg/mapper.html), red arrows representing the proteins found in our study (shotgun and 2D approaches) and green the proteins predicted based on the genome but not experimentally detected.

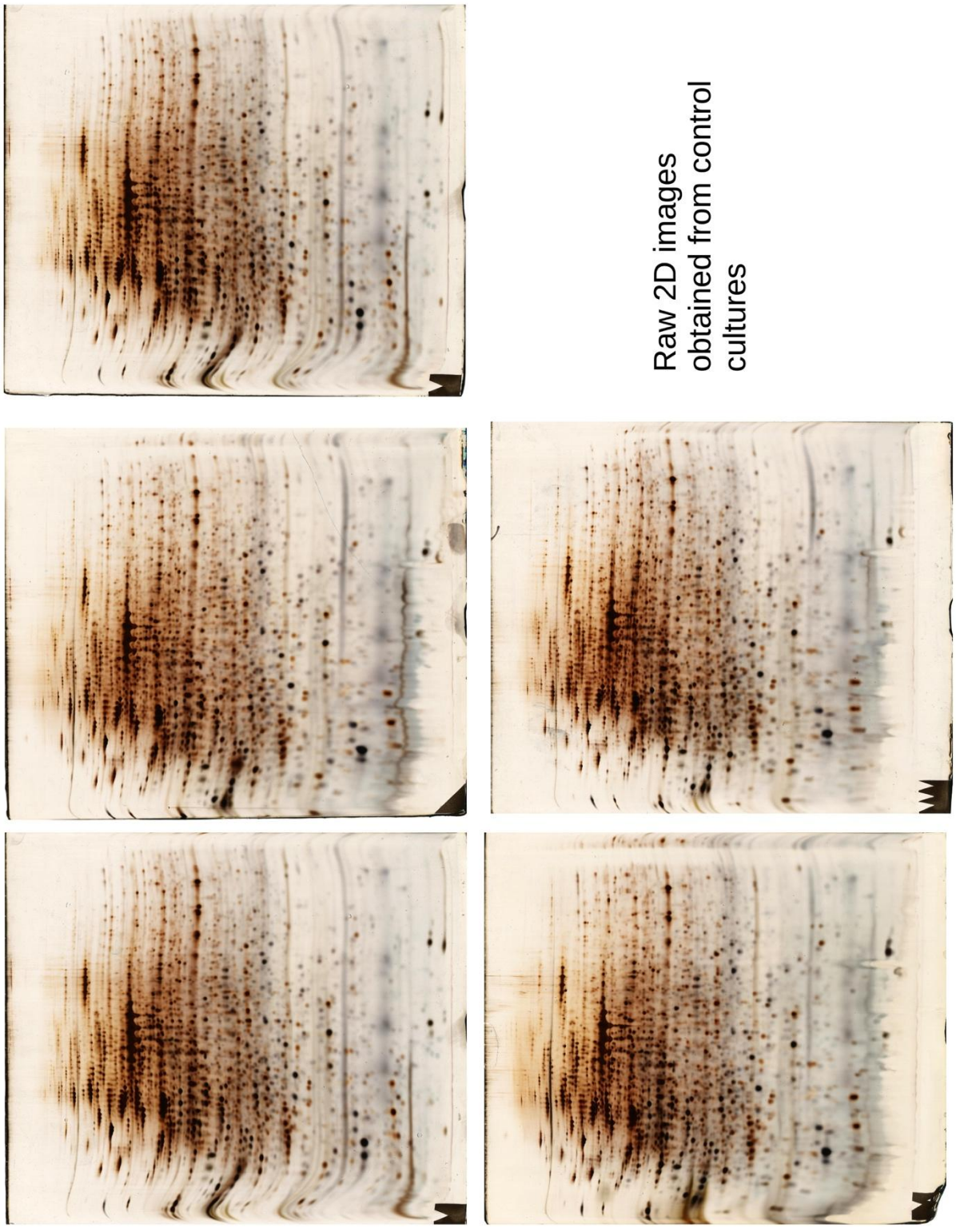

Supplementary Figure 3: Raw 2D images obtained from control cultures

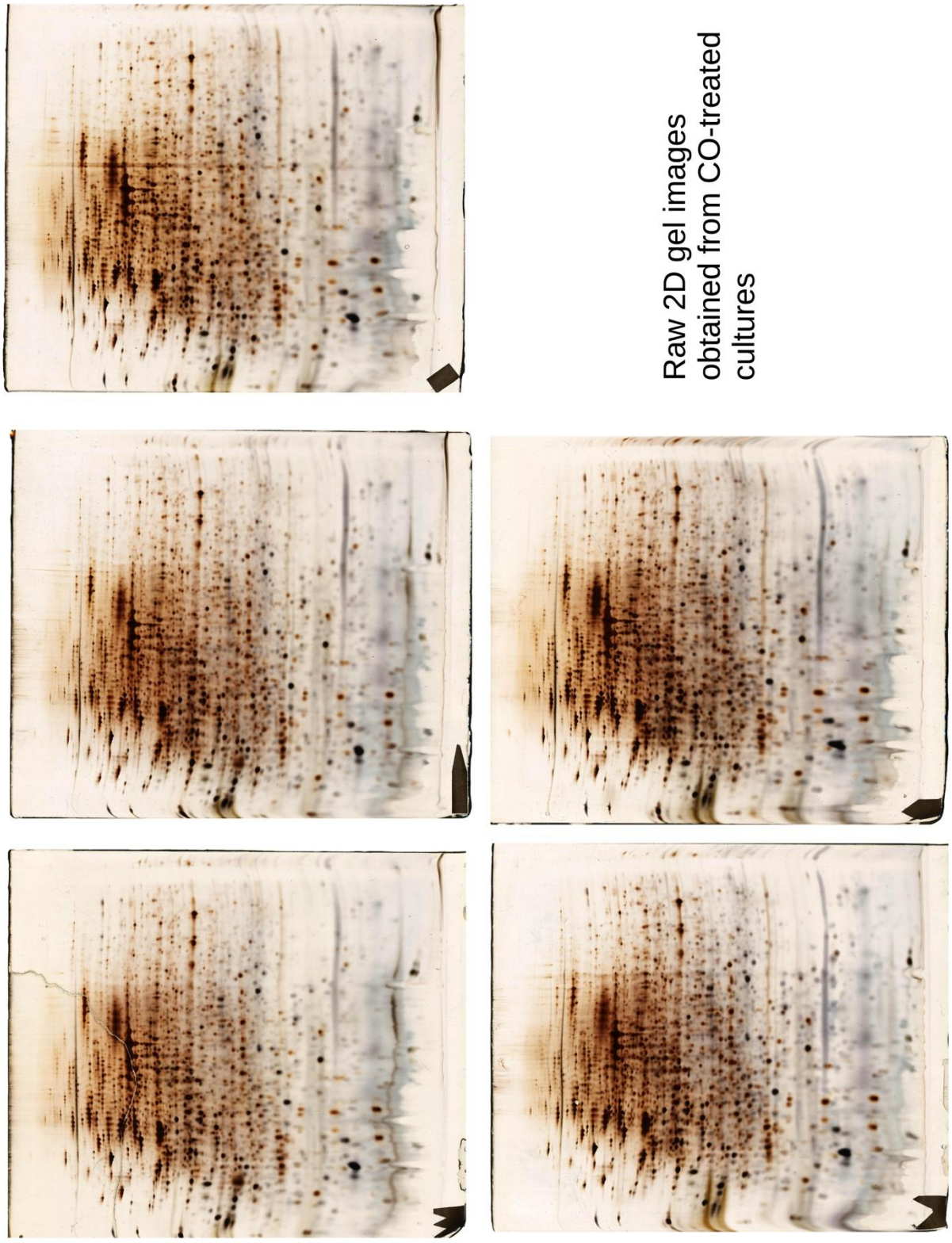

Supplementary Figure 4: Raw 2D images obtained from CO-treated cultures

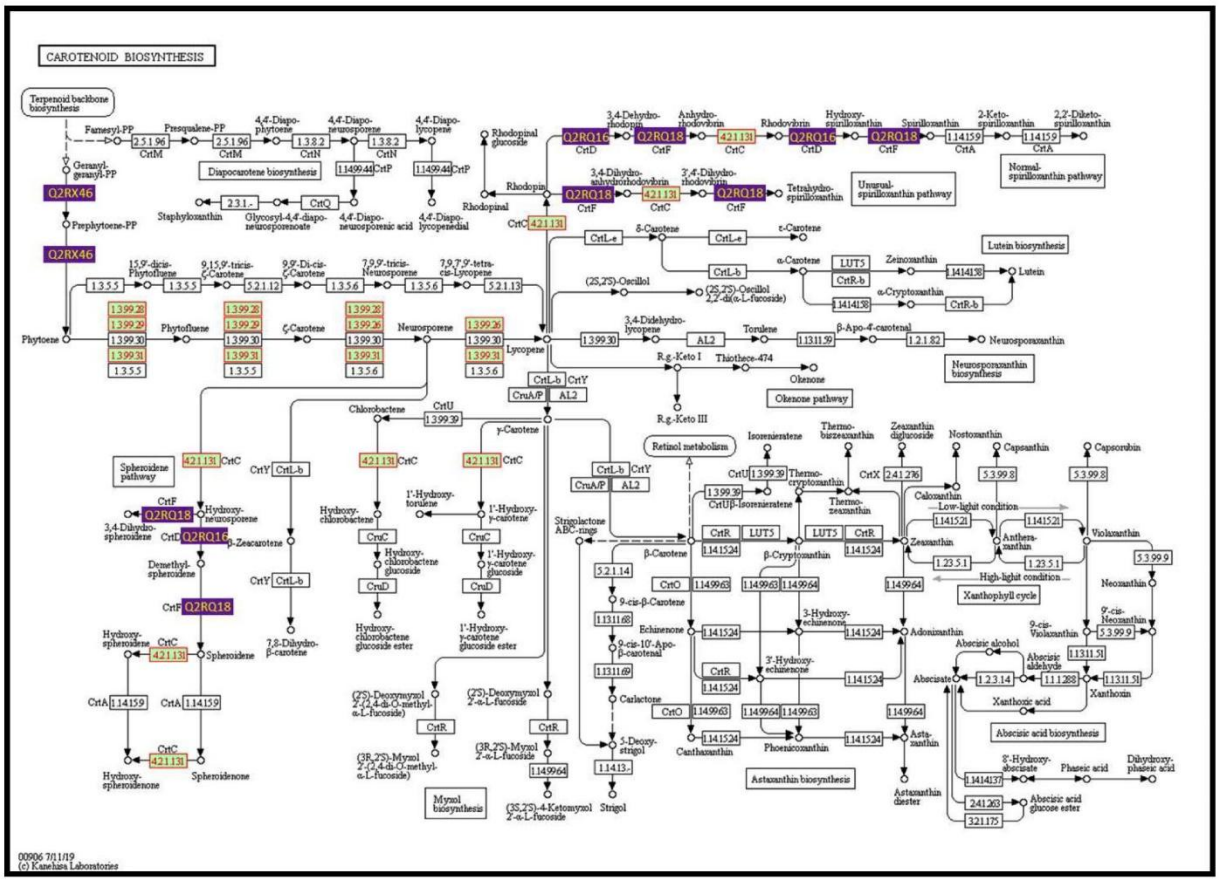

Supplementary Figure 5 : Carotenoid biosynthesis (rru00906)
This figure was made with KEGG mapper (https://www.genome.jp/kegg/mapper.html). Green rectangles represent enzymatic functions to which KEGG program has associated at least one protein from *R. rubrum*; the red borders around the green rectangles indicate that these proteins were identified in our proteome (2D and shotgun approaches). Purple rectangles indicate down-regulated proteins with their uniprot reference.

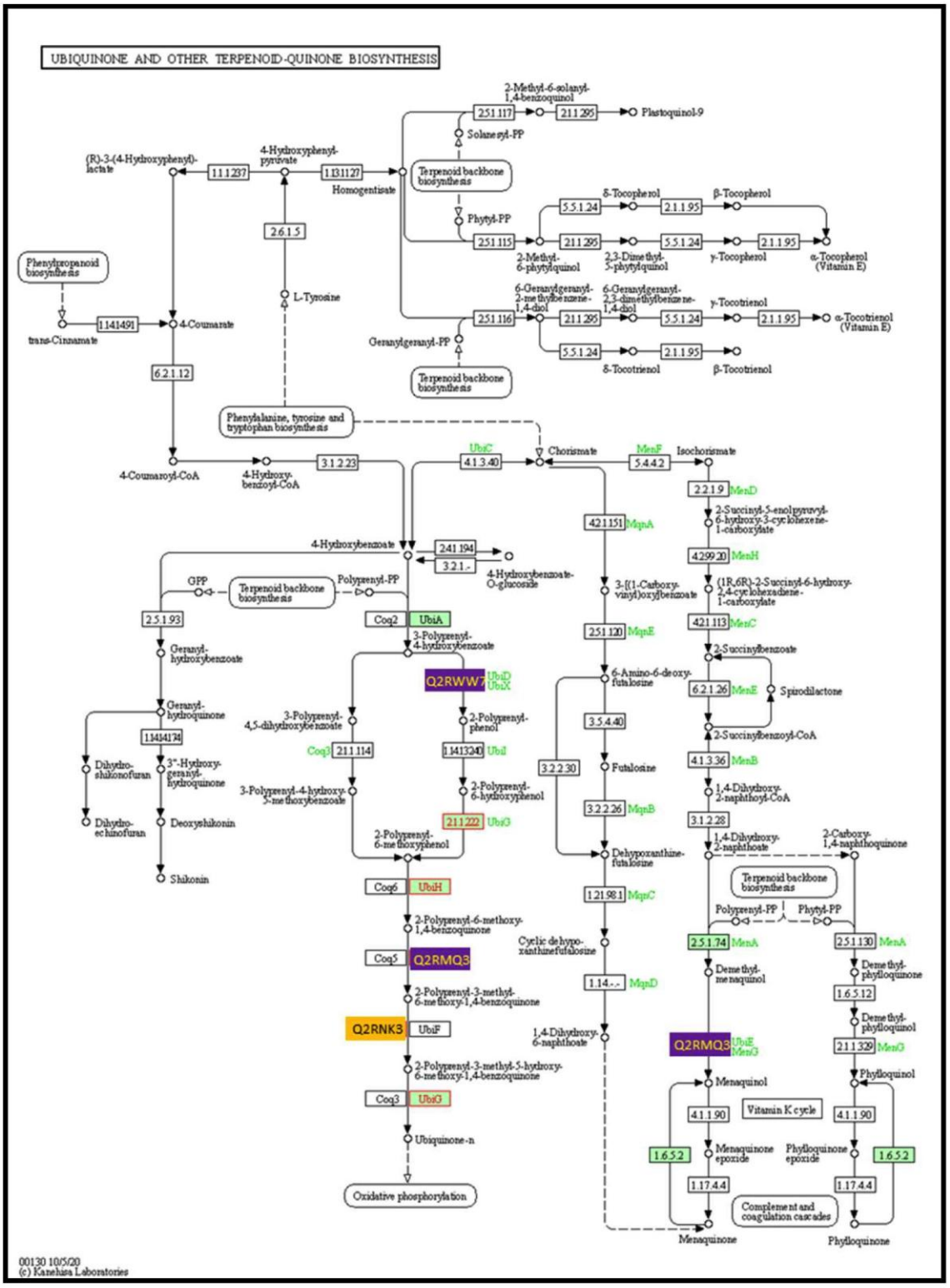

Supplementary Figure 6 : Ubiquinone and other terpenoid-quinone biosynthesis (rru00130)

This figure was made with KEGG mapper (https://www.genome.jp/kegg/mapper.html). Green rectangles represent enzymatic functions to which KEGG program has associated at least one protein from *R. rubrum*; the red borders around the green rectangles indicate that these proteins were identified in our proteome (2D and shotgun approaches). Purple and orange rectangles indicate down-regulated and up-regulated proteins respectively, with their uniprot reference.

.

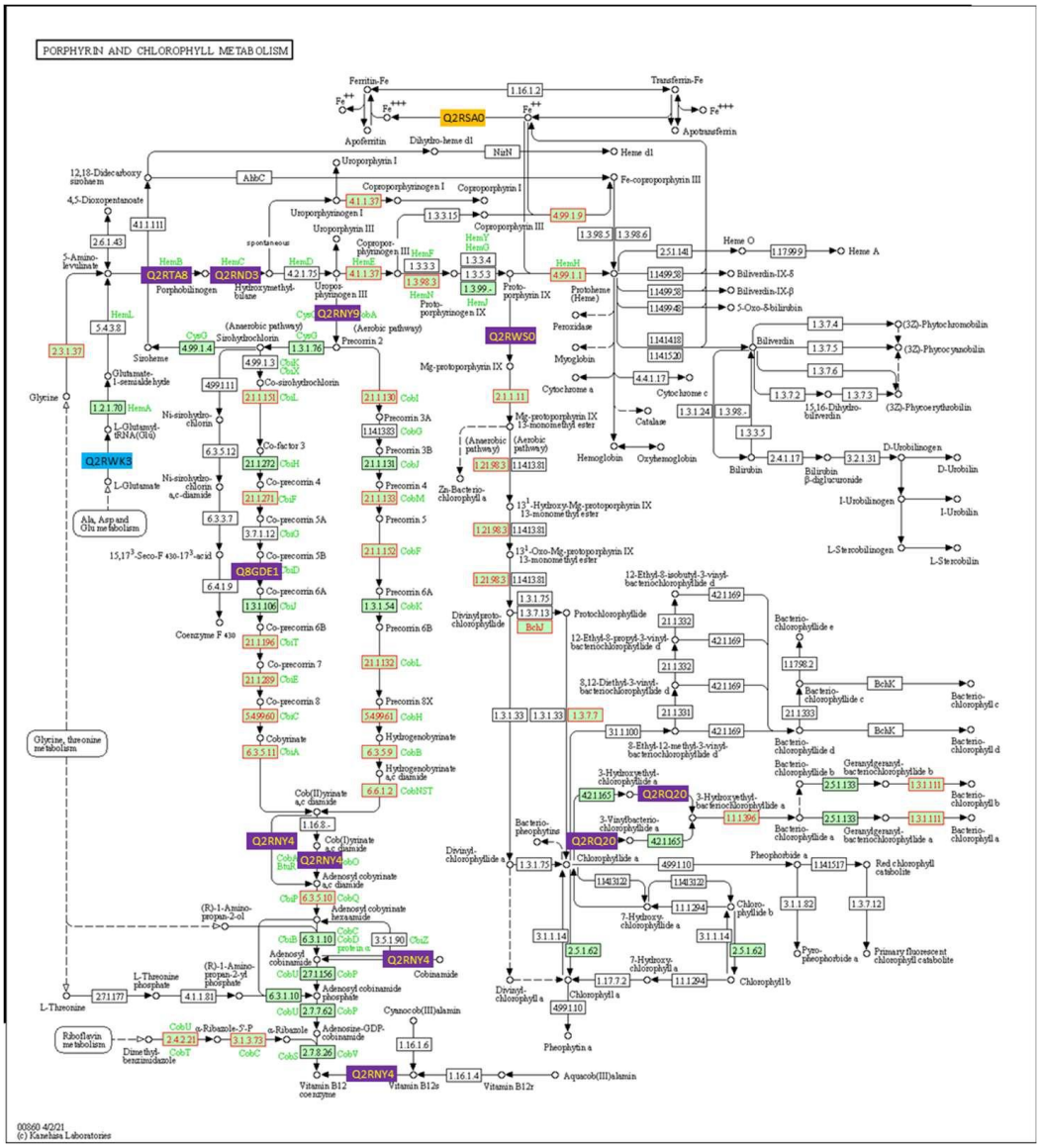

Supplementary Figure 7 : Porphyrin and chlorophyll metabolism (rru00860) This figure was made with KEGG mapper (https://www.genome.jp/kegg/mapper.html). Green rectangles represent enzymatic functions to which KEGG program has associated at least one protein from *R. rubrum*; the red borders around the green rectangles indicate that these proteins were identified in our proteome (2D and shotgun approaches). Purple, orange and cyan rectangles indicate down-regulated, up-regulated, and down-and up-regulated proteins, respectively, with their uniprot reference.

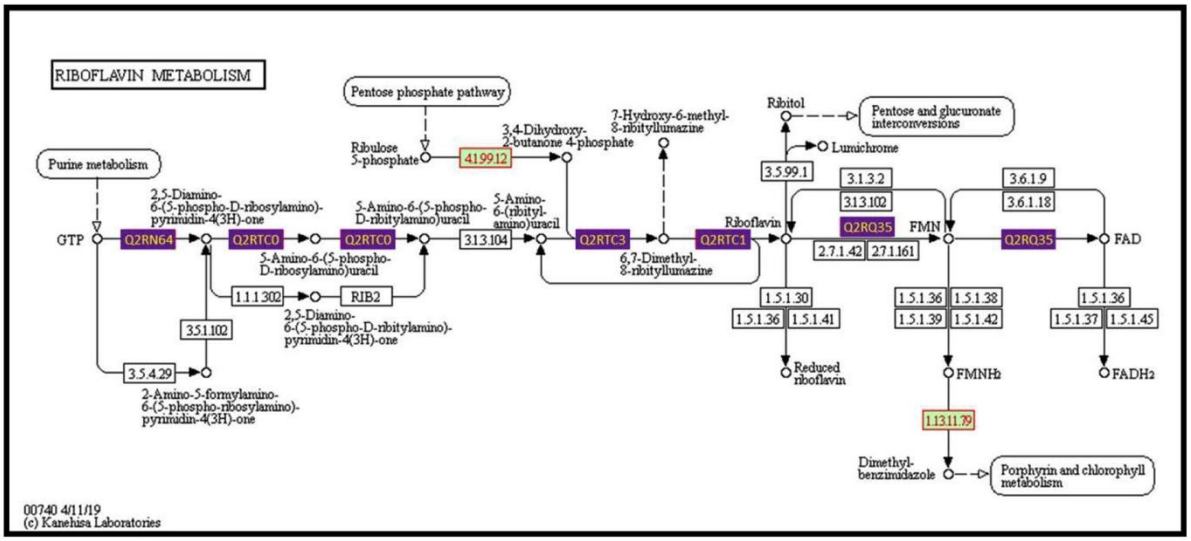

Supplementary Figure 8 : Riboflavin metabolism (rru00740)
This figure was made with KEGG mapper (https://www.genome.jp/kegg/mapper.html). Green rectangles represent enzymatic functions to which KEGG program has associated at least one protein from *R. rubrum*; the red borders around the green rectangles indicate that these proteins were identified in our proteome (2D and shotgun approaches). Purple rectangles indicate down-regulated proteins with their uniprot reference.

Supplementary Figure 9 : Blast and CLUSTAL 2.1 multiple sequence alignment
The Blast search and clustal alignment were performed on KEGG server https://www.genome.jp/tools-bin/blastplus)

Q2RVS7 Versus **CoxM** from *Oligotropha caboxydovorans*

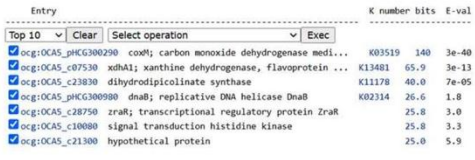

Entry		K number	bits	E-val
ocg:OCA5_pHCG300290	coxM; carbon monoxide dehydrogenase medi...	K03519	140	3e-40
ocg:OCA5_c07530	xdhA1; xanthine dehydrogenase, flavoprotein ...	K13481	65.9	3e-13
ocg:OCA5_c23830	dihydrodipicolinate synthase	K11178	40.0	7e-05
ocg:OCA5_pHCG300980	dnaB; replicative DNA helicase DnaB	K02314	26.6	1.8
ocg:OCA5_c28750	zraR; transcriptional regulatory protein ZraR		25.8	3.0
ocg:OCA5_c10080	signal transduction histidine kinase		25.8	3.3
ocg:OCA5_c21300	hypothetical protein		25.0	5.9

```
Q2RVS7          --MYVFDYHRPNSLADAHGLLTAR-EDAKILAGGMTLIPTLKQRLAQPSDLIDLSACPGL
ocg_OCA5_pHCG300290 MIPGSFDYHRPKSIADAVALLTKLGEDARPLAGGHSLIPIMKTRLATPEHLVDLRDIGDL
                      ******:*:*** .***   ***: **** :*** :* *** *..*:**    .*

Q2RVS7          SGITLAADSLTIGAMTCHAAVAANPQVIAALPALASLAAGIGDPAVRNRGTLGGSIANDD
ocg_OCA5_pHCG300290 VGIREEGTDVVIGAMTTQHALIGSDFLAAKLPIIRETSLLIADPQIRYMGTIGGNAANGD
                     **   . .:.***** : *: .. : * ** : . :  *.** :*  **:**. **.*

Q2RVS7          PAADWPAACLGLGATILTD----SREIAAEDFFLGLFETALEPAEIITAVRFPLP---LA
ocg_OCA5_pHCG300290 PGNDMPALMQCLGAAYELTGPEGARIVAARDYYQGAYFTAIEPGELLTAIRIPVPPTGHG
                    *. * **    ***:        :* :**.*:: * : **:**.*:.**:*:*:*    .

Q2RVS7          AAYAKFDQPASRFALVGVFVARTAAGSRVAVTGASQEGVFRAGDLEKALDRDFSAAALEG
ocg_OCA5_pHCG300290 YAYEKLKRKIGDYATAAAAVVLTMSGGKCVTASIGLTNVANTPLWAEEAGKVLVGTALDK
                     ** *:.:  . :* ... *. * :*.: ..:. .  .* .:    :  .: : .:**:

Q2RVS7          ------VRVSPARLNEDIHGDG--AYRAHLIGVMAGRAVSACQ-----
ocg_OCA5_pHCG300290 PALDKAVALAEAITAPASDGRGPAEYRTKMAGVMLRRAVERAKARAKN
                      * :: *      .* *   **::: ***  ***. .:
```

Q2RVS8 Versus **CoxL** from *Oligotropha caboxydovorans*

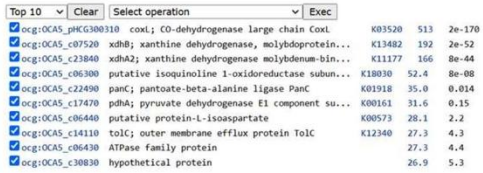

Entry		K number	bits	E-val
ocg:OCA5_pHCG300310	coxL; CO-dehydrogenase large chain CoxL	K03520	513	2e-170
ocg:OCA5_c07520	xdhB; xanthine dehydrogenase, molybdoprotein...	K13482	192	2e-52
ocg:OCA5_c23840	xdhA2; xanthine dehydrogenase molybdenum-bin...	K11177	166	8e-44
ocg:OCA5_c06300	putative isoquinoline 1-oxidoreductase subun...	K18030	52.4	8e-08
ocg:OCA5_c22490	panC; pantoate-beta-alanine ligase PanC	K01918	35.0	0.014
ocg:OCA5_c17470	pdhA; pyruvate dehydrogenase E1 component su...	K00161	31.6	0.15
ocg:OCA5_c06440	putative protein-L-isoaspartate	K00573	28.1	2.2
ocg:OCA5_c14110	tolC; outer membrane efflux protein TolC	K12340	27.3	4.3
ocg:OCA5_c06430	ATPase family protein		27.3	4.4
ocg:OCA5_c30830	hypothetical protein		26.9	5.3

```
Q2RVS8          -MPSDSATVTDLQSAAQRSGIGVSVRRKEDRRFLTGQGTYTDDIVRPGMVHAFLLRSPHA
ocg_OCA5_pHCG300310 MNIQTTVEPTSAERAEKLQGMGCKRKRVEDIRFTQGKGNYVDDVKLPGMLFGDFVRSSHA
                       . :.  *. : * : .*:* . :* ** **  *:*.*.**:  ***:.. ::**.**

Q2RVS8          HARIAALDVGPARAAKGVLAVFTGADMAADKVGSIPCGWAVANKDGTPMAEPPHPALAVD
ocg_OCA5_pHCG300310 HARIKSIDTSKAKALPGVFAVLTAADLKPLNLHYMPT----------LAGDVQAVLADE
                    **** ::*.. *:*  **:**:*.**: . ::  :*          :*   :..** :

Q2RVS8          RVRHVGDAVAVVIARTLAQAKDAAELIEIDYQDLPVVVDPAQALN--------------S
ocg_OCA5_pHCG300310 KVLFQNQEVAFVVAKDRYVAADAIELVEVDYEPLPVLVDPFKAMEPDAPLLREDIKDKMT
                    :* . .: **.*:*:    * ** **:*:**: ***:*** :*::          :

Q2RVS8          PAIHDQAPGNLCYDWEIGDAAAVEAAFARAHHITRLDLINNRLVPNAMEPRSYIGEYDRA
ocg_OCA5_pHCG300310 GAHGARKHHNHIFRWEIGDKEGTDATFAKAEVVSKDMFTYHRVHPSPLETCQCVASMDKI
                     *   :   *  : *****  ..:*:**:*. :::  :  :*: *..:*. . :.. *:

Q2RVS8          TGEYTLTTTSQNPHVIRLLMGAFVLNIPEHKLRVVSPDVGGGFGSKIYHYAEEAIVTWAA
ocg_OCA5_pHCG300310 KGELTLWGTFQAPHVIRTVVSLISG-LPEHKIHVIAPDIGGGFGNKVGAYSGYVCAVVAS
                    .** **  * * ***** :: :   :****::*:.:**:*****.*:  *:  . .. *:

Q2RVS8          PKVGKPIKWTSDRSEAFLSDAHGRDHVSHAELALAEDGTFLALKVDTIANLGAYLSTFST
ocg_OCA5_pHCG300310 IVLGVPVKWVEDRMENLSTTSFARDYHMTTELAATKDGKILAMRCHVLADHGAFDACADP
                      :* *:**..** * : : :..**:   :*** ::**.:**:: ..:*: **: :  ..

Q2RVS8          AVPTYLYATLLAGVYRTPAIHCRVRSVFTNTVP-VDAYRGAGRP-EATYLIERIVDKAAR
ocg_OCA5_pHCG300310 SKWPAGFMNICTGSYDMPVAHLAVDGVYTNKASGGVAYRCSFRVTEAVYAIERAIETLAQ
                    :  .  : .: :* *  *. *  * .*:**...   *** : *  **.* *** ::. *:

Q2RVS8          EIGMDRVALRRKNFIPADAFPYQTPVALQYDSGDYEATLGKALVLADVEGFAARR---AE
ocg_OCA5_pHCG300310 RLEMDSADLRIKNFIQPEQFPYMAPLGWEYDSGNYPLAMKKAMDTVGYHQLRAEQKAKQE
                    .: ** . ** **** .: *** :*:. :****:*  :: **:  .. . : *.:    *

Q2RVS8          AEARG---KVRGLGYSTYLEACGIAPSAVVGSLGARAGLFECAVVRVHPTGSVTVLTGSH
ocg_OCA5_pHCG300310 AFKRGETREIMGIGISFFTEIVGAGPSKNCDILG--VSMFDSAEIRIHPTGSVIARMGTK
                    *  **   :: *:* * : *  * .**   . **  ..:*:.* :*:****** .  *::

Q2RVS8          SHGQGHETTFAQLVSDTLGLPIENVEISHGDTNKVPFGMGTYGSRSLAVGGEALMKAMGK
ocg_OCA5_pHCG300310 SQGQGHETTYAQIIATELGIPADDIMIEEGNTDTAPYGLGTYGSRSTPTAGAATAVAARK
                    *:*******:**:::  **:* ::: *..*:*:..*:*:******* ...* *   *  *

Q2RVS8          VVDKARKIAAHALEAAVEDVEFKDGSFTIAGTDKAMTFAQVALTAYVPHNFPHDQLEPGL
ocg_OCA5_pHCG300310 IKAKAQMIAAHMLEVHEGDLEWDVDRFRVKG--LPEKFKTMKELAWASYNSPPPNLEPGL
                    :  **: **** **.   *:*:. . * : *   . .*  :   *:..:* *  :*****

Q2RVS8          EEQAFYDPMNFTYPGGCHICEVEIDPQTGVVEVVAMTAVDDVGRVINPMIVHGQIHGGLA
ocg_OCA5_pHCG300310 EAVNYYDPPNMTYPFGAYFCIMDIDVDTGVAKTRRFYALDDCGTRINPMIIEGQVHGGLT
                    *   :*** *:*** *.::* ::** :***.:.  : *:** *  *****:.**:****:

Q2RVS8          QGIGQALIEGCAYDANGQLVTGSFMDYAMPRADRLPSFRVDNAVTLCAHNSLGVKGCGEV
ocg_OCA5_pHCG300310 EAFAVAMGQEIRYDEQGNVLGASFMDFFLPTAVETPKWETDYTVTPSPHHPIGAKGVGES
                    :.:. *: :   ** :*::: .****: :* * . *.:.:* :** ..*:.:*.** **

Q2RVS8          GAIGSPPAVINAVLDALAPLGVSDIAMPATPFRVWRAIEAARAAAQ
ocg_OCA5_pHCG300310 PHVGGVPCFSNAVNDAYAFLNAGHIQMPHDAWRLWKVGEQLGLHV-
                      :*. *.. *** ** * *....* **  .:*:*:. *     .
```

Q2RVS9 Versus **CoxS** from *Oligotropha caboxydovorans*

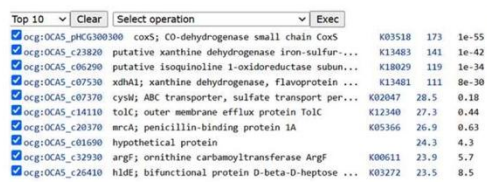

Entry		K number	bits	E-val
ocg:OCA5_pHCG300300	coxS; CO-dehydrogenase small chain CoxS	K03518	173	1e-55
ocg:OCA5_c23820	putative xanthine dehydrogenase iron-sulfur-...	K13483	141	1e-42
ocg:OCA5_c06290	putative isoquinoline 1-oxidoreductase subun...	K18029	119	1e-34
ocg:OCA5_c07530	xdhA1; xanthine dehydrogenase, flavoprotein ...	K13481	111	8e-30
ocg:OCA5_c07370	cysW; ABC transporter, sulfate transport per...	K02047	28.5	0.18
ocg:OCA5_c14110	tolC; outer membrane efflux protein TolC	K12340	27.3	0.44
ocg:OCA5_c20370	mrcA; penicillin-binding protein 1A	K05366	26.9	0.63
ocg:OCA5_c01690	hypothetical protein		24.3	4.3
ocg:OCA5_c32930	argF; ornithine carbamoyltransferase ArgF	K00611	23.9	5.7
ocg:OCA5_c26410	hldE; bifunctional protein D-beta-D-heptose ...	K03272	23.5	8.5

```
Q2RVS9          --MPMVSMTVNGEVVSGEVETRTLLVDFLRHTLGLTGTHVGCDTSQCGACVIHMNGVAVK
ocg_OCA5_pHCG300300 MAKAHIELTINGHPVEALVEPRTLLIHFIREQQNLTGAHIGCDTSHCGACTVDLDGMSVK
                      . :.:*:**. *.. **.****:.*:*.  .***:*:*****:****.:.::*:.:**

Q2RVS9          SCSVLTVMAEGAEILTIEGLSGNGPGDALHPMQEAFREHHGLQCGFCTPGMVMTALDLVA
ocg_OCA5_pHCG300300 SCTMFAVQANGASITTIEGMAA--PDGTLSALQEGFRMMHGLQCGYCTPGMIMRSHRLLQ
                    **:::* *:**.* ****::.  *..:* .:**.**  ******:*****:* : *:

Q2RVS9          RDPDPDEAAIRRGLEGNICRCTGYHNIVKAVREGASRLREAGRAAAQ-
ocg_OCA5_pHCG300300 ENPSPTEAEIRFGIGGNLCRCTGYQNIVKAIQYAAAKINGVPFEEAAE
                    .:*.* ** ** *: **:******:*****:: .*:::. .    *
```